

Submarine Groundwater Discharge and Hypoxia: Lessons Learned from an
Estuary in the Semi-arid Area of South Texas

A Thesis

by

WILLIAM A. MCBEE

MASTER of SCIENCE

In

ENVIRONMENTAL SCIENCE

Texas A&M University-Corpus Christi
Corpus Christi, Texas

DECEMBER 2017

© WILLIAM ALEXANDER MCBEE II

All Rights Reserved

DECEMBER 2017

Submarine Groundwater Discharge and Hypoxia: Lessons Learned from an
Estuary in the Semi-arid Area of South Texas

A Thesis

by

WILLIAM A. MCBEE

This thesis meets the standards for scope and quality of
Texas A&M University-Corpus Christi and is hereby approved.

DR. DORINA MURGULET
Chair

DR. MICHAEL WETZ
Committee Member

DR. VALERIU MURGULET
Committee Member

ABSTRACT

Formations of hypoxia in Corpus Christi Bay (CCB) and algal blooms in the Upper Laguna Madre have become a concern as they have cyclically surfaced during the late spring through the fall months. The semi-arid climate of South Texas experiences limited precipitation and surface freshwater inflows, which in turn would point to non-riverine sources such as groundwater as a contributor to the overall nutrient budget. Groundwater has a tendency to accumulate high concentrations of nutrients and organic matter. Despite the potential impact that submarine groundwater discharge (SGD, including groundwater discharge and sediment fluxes) has on estuary systems worldwide, this input has not been well understood. The objective of this study is to use a combination of geophysical and geochemical techniques to enhance the understanding of spatial and temporal occurrence of SGD and related nutrient fluxes and the effects of these inputs on the hypoxia formation in a semiarid estuarine system. Results from multiple continuous electrical resistivity (ER) profiles, spanning from near shore to 2 km offshore, were used to characterize subsurface hydrogeologic heterogeneity and select sampling sites for nutrient and SGD analyses during three seasonal events (winter, summer, and fall). SGD measurements were conducted at three locations using both continuous ER and radon measurements. During summer and late fall, SGD rates show large spatial variances, with the highest average discharge rates measured at the Oso Bay (a secondary bay) inlet ($13.1 \text{ m}^3/\text{m}\cdot\text{d}$), followed by Shamrock Island ($2.6 \text{ m}^3/\text{m}\cdot\text{d}$) and Laguna Madre inlet ($1.1 \text{ m}^3/\text{m}\cdot\text{d}$). On average, SGD rates were higher during late fall ($6.5 \text{ m}^3/\text{m}\cdot\text{d}$) than summer ($4.7 \text{ m}^3/\text{m}\cdot\text{d}$). As a result of higher SGD rates and more enriched nutrient levels in porewater, nutrient fluxes during fall are one order of magnitude higher than summer. Based on the good spatial correlation between dissolved oxygen levels and high ^{222}Rn -derived nutrient fluxes, this study indicates that SGD is

not only a significant contributor to the nutrient budget but there is also a possible correlation between these inputs, algal blooms, and hypoxia.

TABLE OF CONTENTS

Abstract	i
Table of Contents	iii
List of Figures	v
List of Tables	vii
1. Introduction	1
1.1. Background	1
1.2. Study Site	3
1.2.1. Physiographic Aspects	4
1.2.2. Soils.....	6
1.2.3. Hydrogeology	7
2. Methods.....	8
2.1. Sampling Design	8
2.2. Resistivity Imaging.....	9
2.2.1. Data Collection.....	9
2.2.2. Salinity Mass Balance and Submarine Groundwater Discharge	13
2.3. Radon Submarine Groundwater Flux Calculations.....	15
2.4. Nutrient and Chlorophyll-a Sampling.....	20
3. Results and Discussion	20
3.1. Continuous Resistivity Profiles.....	20
3.2. Time-Lapse Resistivity Profiling and Resistivity-Derived SGD Rates	26
3.3. Radon-derived Submarine Groundwater Discharge Rates.....	35

TABLE OF CONTENTS

3.4. Nutrient Fluxes and the Presence of Chlorophyll-a.....	40
3.5. Spatial and Temporal Extent of Hypoxia.....	46
4. Summary	49
5. Literature Cited.....	53
6. Appendix.....	61
6.1. Nutrient Data.....	61

List of Figures:

Figure 1: Study Site	5
Figure 2: Soils	7
Figure 3: Super Sting R8 Marine	11
Figure 4: RAD7	16
Figure 5: Box Model	19
Figure 6: CRP-Laguna Madre	23
Figure 7: CRP-Oso Inlet.....	23
Figure 8: CRP-Laguna Mouth	24
Figure 9: CRP-Shamrock Island	24
Figure 10: CRP-University Beach	25
Figure 11: Rainfall	26
Figure 12: Time-Lapse Oso Inlet-Summer	29
Figure 13: Time-Lapse Oso Inlet-Fall	30
Figure 14: Time-Lapse Laguna Mouth-Summer.....	31
Figure 15: Time-Lapse Laguna Mouth-Fall.....	32
Figure 16: Time-Lapse Shamrock Island-Summer	33
Figure 17: Time-Lapse Shamrock Island-Fall	34
Figure 18: SGD and Radon Flux Rates	37
Figure 19: Summer Nutrient Concentrations.....	40
Figure 20: Fall Nutrient Concentrations.....	40
Figure 21: Summer Nutrient Fluxes	42
Figure 22: Fall Nutrient Fluxes	42
Figure 23: Total Nutrient Fluxes	43

Figure 24: Winter DOC/Chlorophyll-a	44
Figure 25: Summer DOC/Chlorophyll-a.....	45
Figure 26: Fall DOC/Chlorophyll-a.....	45
Figure 27: DO Bottom Spatial Map	47
Figure 28: DO Water Column Average Spatial Map	48

List of Tables:

Table 1. Estimated Flux and Submarine Groundwater Discharge Rates	36
Table 2. Oso Nutrient Comparison	43
Table N6-1. Summer Nutrient Concentrations	61
Table N6-2. Fall Nutrient Concentrations	61
Table N6-3. Summer Nutrient Flux Estimates	61
Table N6-4. Fall Nutrient Flux Estimates	62
Table N6-5. Total Nutrient Flux Concentrations Summer/Fall	62

1. Introduction

1.1. Background

Submarine groundwater discharge (SGD) is the outflow of groundwater across the ocean-land interface into oceans, bays, or estuaries (Church, 1996). SGD is primarily controlled by hydraulic gradients from inland watersheds and coastal boundaries driving groundwater and seawater through sediments, though other gravitational, oceanic tidal, and dispersive circulation forces act on the freshwater and saltwater interface within the coastal aquifers (Mulligan & Charette, 2005). Shallow unconfined aquifers are subject to recharge in close proximity to coastal embayments, whereas recharge for deeper confined aquifers can occur long distances inland from the coast (Mulligan & Charette, 2005). Thus, contaminants from a vast array of sources can ultimately discharge into the coastal system. Similar to surface inflows, SGD plays an important role in the vitality and health of coastal and estuarine waters by providing fresh or less saline water, nutrients, and other harmful or necessary inputs.

Typically groundwater contains higher nutrient levels than rivers, streams, and the receiving seawater (Church, 1996). Anthropogenic inputs of nutrients (from sources such as fertilizers, pesticides, faulty septic tanks) have been shown to provide aquifers with nutrients (nitrogen, phosphate, potassium, etc.) and other contaminants (Rajmohan & Elango, 2005). High concentrations of organic matter tend to accumulate in groundwater (Church, 1996), mainly through infiltration from land surface sources in outcrop areas. Organic matter-contaminated groundwater discharging to the bays may fuel bacterial respiration, leading to hypoxia formation. It has also been demonstrated that nutrient-contaminated groundwater can fuel growth of phytoplankton and algae in coastal systems (Church, 1996). Eutrophication is a potential result

of increased nutrient concentration in coastal waters that could be derived from groundwater (Selman *et al.*, 2008).

Commonly, multiple methods have been utilized to investigate the contribution of groundwater to surface water such as numerical modeling (Guo and Langevin, 2002; Murgulet and Tick, 2015), geochemical tracers (Cable *et al.*, 2004; Ni *et al.*, 2011), and statistical methods (Morehead *et al.*, 2008; Thareja *et al.*, 2011). Recently, subsurface imaging techniques, such as direct current electrical resistivity (ER) surveys have been increasingly used to delineate and quantify groundwater flow paths and discharge rates into surface water bodies (White, 1988; Greenwood *et al.*, 2006; Green *et al.*, 2008; Nyquist *et al.*, 2008; Cardenas *et al.*, 2010; Dimova *et al.*, 2012). Consecutive/continuous ER images acquired along the same survey lines over time periods of hours or during different environmental conditions are used to locate potential groundwater discharge seepage faces and estimate changes in discharge rates over time (Nyquist *et al.*, 2008; Dimova *et al.*, 2012; Johnson *et al.*, 2012).

In addition, applications of radon (^{222}Rn ; half-life ($t_{1/2}$)=3.8 d) as a geochemical tracer has proven to be successful in estimation of SGD rates (Moore 1996; Burnett and Dulaiova, 2003). However, very few studies have employed this method in combination with ER imaging. Radon, a naturally occurring inert gas commonly found in soils and subsurface sediments/rocks and the product of Radium (Ra) decay (Figure 1) (Crusius *et al.*, 2005), is abundant in groundwater in relation to surface waters (Burnet and Dulaiova, 2003). Therefore, these properties make radon an ideal tracer of groundwater discharge in coastal waters. However, studies relying solely on geochemistry tracers do not provide a comprehensive understanding of groundwater sources, as measured fluxes of any given constituent/tracer will only offer a total groundwater discharge rate, which could include both recirculated water and land-derived SGD (Li *et al.*, 2009).

This study aims to address not only the link between coastal hypoxia and SGD-derived nutrients and organic matter, but to advance scientific understanding of coastal hydrologic heterogeneity and the associated impacts on spatial and temporal occurrence of SGD. To that end, this study utilizes a combination of electrical resistivity, radon, radium, and nutrient data to quantify the SGD derived nutrient inputs but also better understand the effects of these inputs on the bay system as it pertains to hypoxia and harmful algal blooms. This study uses Corpus Christi Bay, located in the semi-arid area of South Texas, as a case study to demonstrate the feasibility of the proposed methodology. The following section describes the relevance of using Corpus Christi Bay area for this proposed study.

1.2. Study Site

The South Texas Gulf Coast is comprised of an extensive network of intracoastal waterways and bay systems. These systems, shielded by Padre Island, provide a unique habitat for a variety of commercially and recreationally important fish and shellfish species, marine mammals, reptiles, resident birds, shorebirds, and other avian species. Corpus Christi Bay, Oso Bay, and the upper Laguna Madre are experiencing annual formations of hypoxia, characterized by dissolved oxygen (DO) levels less than 2 mg/L and brown tide, as well as, red tide events in the past three decades ([Nelson & Montagna, 2009](#)). The Corpus Christi area saw a 2.3% population increase between 2010 and 2012 ([U.S. Census Bureau, 2014](#)), and with increases in population and the growing demand on regional resources due to tourism, nutrient and organic matter loading to both aquifers and surface waters from point and non-point sources is expected to increase, thus contributing to water quality degradation ([Krothe et al., 2002](#)).

Reoccurring formations of hypoxia have cyclically occurred during the late spring through the fall months in Corpus Christi Bay ([Nelson & Montagna, 2009](#)). Due to the semi-arid climate of

the south Texas Gulf Coast, estuaries receive minimal surface freshwater inflows due to limited precipitation, which point to non-riverine sources as influential contributors of nutrients and organic matter. Various coastal systems around the world have experienced and recorded water quality degradation due to nutrient loading from groundwater that can fuel phytoplankton growth, as well as, bacterial respiration aiding in hypoxic episodes (Church, 1996).

A wealth of studies have investigated the relationship between the formation of hypoxia and nutrient levels (Turner et al., 2008), but no studies have addressed the groundwater component in nutrient and freshwater budgets in Corpus Christi Bay. Corpus Christi Bay (CCB) plays an important role, environmentally and economically, to the surrounding area, and despite the potential importance of SGD to the nutrient budget and overall vitality of the surrounding coastal waters, SGD has been overlooked. This multi-method study shows that in order to effectively quantify and evaluate the nutrient fluxes and budgets to coastal embayments, a comprehensive understanding of SGD and the associated solute inputs is necessary.

1.2.1. Physiographic Aspects

Study sites were selected along an area ranging from the Upper Laguna Madre (ULM) to the southern half of Corpus Christi Bay (CCB) (Figure 1), predominantly shielded from the Gulf of Mexico by North Padre Island. The surface area of Corpus Christi Bay is roughly 445 km² and represents approximately 7.1% of the overall Texas estuary network (USEPA, 1999). Corpus Christi Bay is a shallow (~3.2 m; Orlando et al. 1991), almost enclosed bay with a level bottom (Montagna and Kalke 1992; Martin and Montagna 1995; Ritter and Montagna 1999) and a total open water surface area of 432.9 km². Given the microtidal (small tidal range) characteristic, this bay is sensitive to meteorological forces such as temperature, precipitation, and wind. Average monthly wind speeds range from 17 km/h to 28 km/h, and two principle wind regimes

dominate the Corpus Christi Bay: persistent, southeasterly winds from March through September and north-northeasterly winds from October through March (Behrens and Watson 1973; Brown *et al.* 1976).

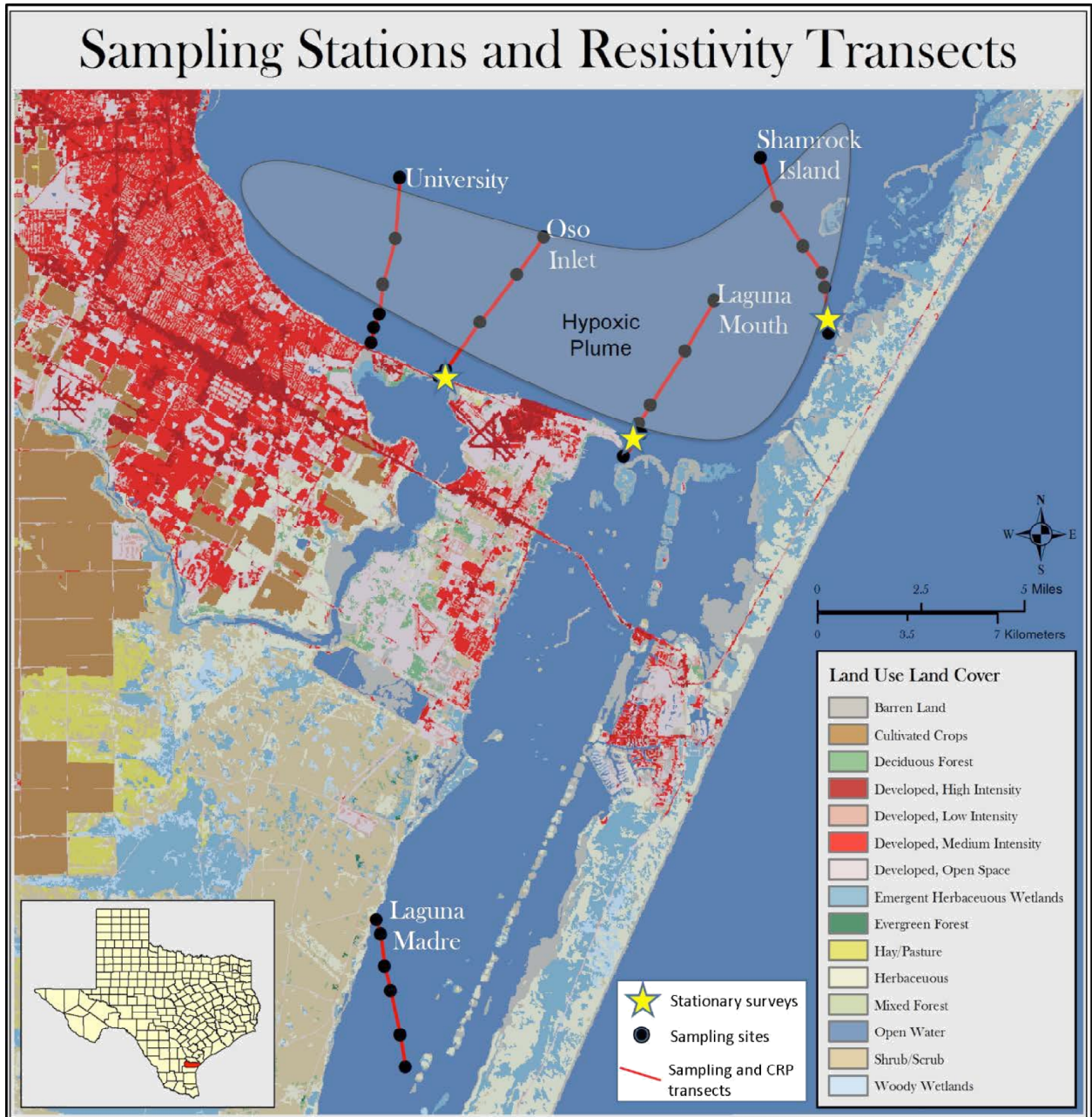


Figure 1: Study site, sampling transects, and sampling stations.

Corpus Christi Bay is connected with several bodies of water including Oso Bay, Nueces Bay, Aransas Bay, and the Gulf of Mexico due to dredged ship channels and canals and natural hydrological process. These secondary bays and the Gulf provide the system with a mix of saline and freshwater, as well as, an influx of nutrients; however, Oso Bay is assumed to be the primary nutrient input into CCB because of the large discharges from municipal wastewater treatment plants. The mean depth of Corpus Christi Bay is 2.4 m, whereas the Upper Laguna Madre has a mean depth of 1.2 m. Prevailing southeastern winds drive the shallow waters, resulting in a generally well-mixed water column during the fall and winter and a more stratified water column during the late-spring and summer months due to increased temperatures (Verity et al., 2006).

1.2.2. Soils

Nueces County is comprised of eight unique soil compositions, three of which come in contact with and/or overly the Corpus Christi Bay and the Upper Laguna Madre: Victoria Association, Orelia-Banquete Association, and Galveston-Mustang Tidal Flats Association (Figure 2) (USDA, 1992). The Victoria Association soils are dark-gray, calcareous heavy clays with slow infiltration rates. The Orelia-Banquete soils are comprised mostly of a thin sandy surface layer overlaying a large clay layer, with slow infiltration rates. In contrast, the Galveston-Mustang Tidal Flats soils form a surface layer of light-gray fine sand with small amounts of humus with subsoil composed of light-grey fine grain sand commonly saturated with water (USDA, 1992). The Galveston soils are in contact with majority of Corpus Christi Bay and the Upper Laguna Madre but are generally imbedded within large Beaumont clay formations (see section on hydrogeology). The fine-grained sands of the Galveston soils could potentially act as potential conduits for shallow groundwater transport and discharge to Corpus Christi Bay and the Upper

Laguna Madre.

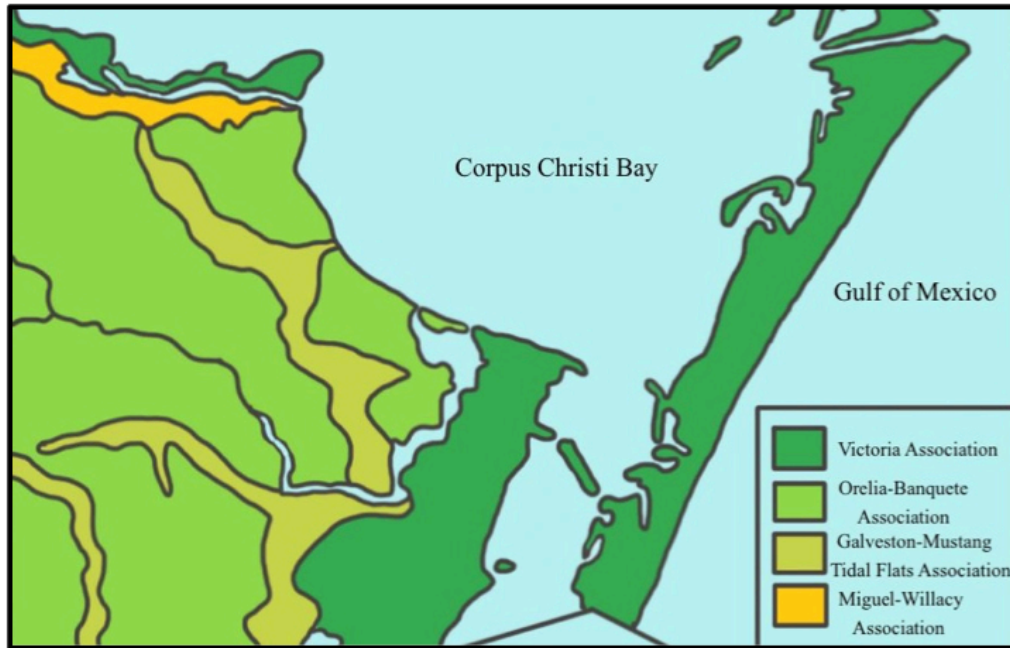


Figure 2. Soil composition of Corpus Christi Bay and the surrounding barrier island (USDA, 1992).

1.2.3. Hydrogeology

The Gulf Coast Aquifer is a leaky artesian aquifer comprised of a complex of clays, silts, sands, and gravels (Ashworth and Hopkins, 1995) that form the Chicot, Evangeline, and Jasper aquifers (Waterstone *et al.*, 2003). Corpus Christi Bay and the surrounding systems are generally in direct contact with the Chicot aquifer, which is the shallowest of the aforementioned aquifers. The stratigraphic units of the Chicot aquifer consist of an overlying alluvial formation preceded by Beaumont and Lissie formations (Ashworth and Hopkins, 1995), which are generally composed of clays and clayey silts with intermittent sand and gravel lenses that continue out into the Gulf of Mexico (Waterstone *et al.*, 2003). The sandy and gravel lenses and dredged channels

within the investigated system provide conduits for SGD despite the potentially limiting clay/impermeable formations.

2. Methods

2.1. Sampling Design

Five sampling transects were selected within Corpus Christi Bay and the Upper Laguna Madre: transect T1-Laguna Madre; Transect T2-Oso Bay Inlet; Transect T3-Laguna Madre Inlet/Mouth; Transect T4-Shamrock Island; and Transect T5-University Beach (Figure 1). Water samples from porewater and water column were collected from six sampling sites placed along each transect, spanning 2 km from near shore to offshore (Figure 1). Transects were selected within the area reported to be affected by hypoxia and areas with significant external input such as discharge from Oso Bay (discharge points) and outputs such as the Laguna Madre mouth. Surface water and porewater samples were analyzed for nutrients such as dissolved organic carbon (DOC), total dissolved nitrogen (TDN), ammonium (NH₄), nitrite and nitrate (NO_x), orthophosphate (o-phosphate), silicate (porewater and surface water) and chlorophyll-a (surface water).

Water samples and electrical resistivity (ER) data were collected during three seasons (i.e. winter, summer and fall of 2014) to capture groundwater discharge rates, nutrient, and biomass distribution under different environmental conditions. Sampling techniques for water column and porewater comply with standard sampling techniques ([Brown *et al.*, 1970](#); [Wood, 1976](#); [RCRA SOP, 2009](#)). At each location, the water depth was measured using a secchi disc. Samples from the water column were collected in increments of 0.5 m with a maximum of three samples from the water column, depending on bathymetry. Field parameters (pH, conductivity, salinity, and DO) were measured before sample collection using an YSI multiparameter water quality meter.

Prior to and following completed field sampling the YSI was calibrated using Hach standards via the YSI guidelines and recorded in a digital spreadsheet. The YSI meter was placed at each sampling depth within the water column for several minutes to allow proper circulation of sample and instrument stability before parameters were recorded.

Surface water samples were collected using a Van Dorn water sampler, deployed to each sampling depth. Sampling bottles were rinsed three times and then overfilled, capped, and placed on ice depending on the required procedure for each analyte. A porewater sampler (AMS Retract-a-Tip) was used to collect porewater samples. The porewater sampler consists of 1 m sections of hollow steel pipe attached to a retract-a-tip point that is injected about 0.2 to 1 m below the sediment-water interface. The injection depth is critical to sampling, to isolate porewater from bottom water intrusion ([RCRA SOP, 2009](#)). Silicone tubing is ran inside the steel pipe and attached to the retract-a-tip on one end and a peristaltic pump on the other. The silicone tubing is purged to three times its volume or until it is free of any sediment. All samples collected are stored at 4 degrees (°C) until analyzed.

2.2. Data Collection

2.2.1. Resistivity Imagining

The project began with a reconnaissance survey within the area reported to be affected by hypoxia and areas with external input such as discharge from Oso Bay (discharge points) and outputs such as the Laguna Madre mouth. Continuous resistivity profiling (CRP) conducted using a continuous injection of current along a moving path were used as reconnaissance tools to help delineate areas of interest revealed by measured resistivity anomalies. Three locations were selected from the CRP images to perform stationary time-lapse resistivity imaging. These locations showed significant signs of interaction between the subsurface interstitial fluid and

water column. Time-lapse inversions were collected during the July and November/December sampling events and thus captured subsurface changes during different environmental conditions, tide cycles, and transitions in wet and dry seasons. Time-lapse images were collected with the resistivity cable deployed along the bottom of the bay and sequentially captured images throughout a 6-8 hour span in attempt to capture the groundwater discharge during a tidal cycle. The individual electrical resistivity images were then compiled into a continuous dataset or tomograph and inverted to earth model resistivity values using the 2D AGI EarthImager with a maximally smooth least squares algorithm (Samouëlian et al., 2005).

Electrical resistivity imaging of the subsurface and water column has shown promise in providing a visual representation of the interactions between surface waters and potential conduits of SGD (Nyquist *et al.*, 2008). These surveys can be used to characterize the subsurface hydrostratigraphy and heterogeneity by constraining rock and soil formations using common resistivity values (Nyquist *et al.*, 2008). The theoretical premise of using ER surveys is based on the induction of direct electric current from the ground surface to create an image of the subsurface using resistivity distribution. Several parameters must be considered when measuring the subsurface resistivity, including the mineral and fluid conductivity, porosity, and water saturation of the rock and/or clay (Loke, 2011). Marine profiles (i.e. continuous resistivity profiles-CRP), which are continuous resistivity measurements of the water column and the subsurface sediments, are complemented by GPS positioning and depth profiles allowing for a greater level of precision in data interpretation.

The resolution of subsurface materials acquired using ER imaging systems is much higher than those of other geophysical methods (Doll *et al.*, 2012). This is not to claim that there are not uncertainties associated with electrical resistivity data inversions, but the ability to measure

larger variances in resistivity facilitate a greater visual interpretation of subsurface sediments, bedrocks minerals, and interstitial fluids (Dimova et al., 2012). Furthermore, the increased resolution of the ER inversions capture changes in porewater resistivity and aquifer substrate-related characteristics on land and offshore (given a relatively shallow water depth) (Viso et al., 2010; Dimova et al., 2012).

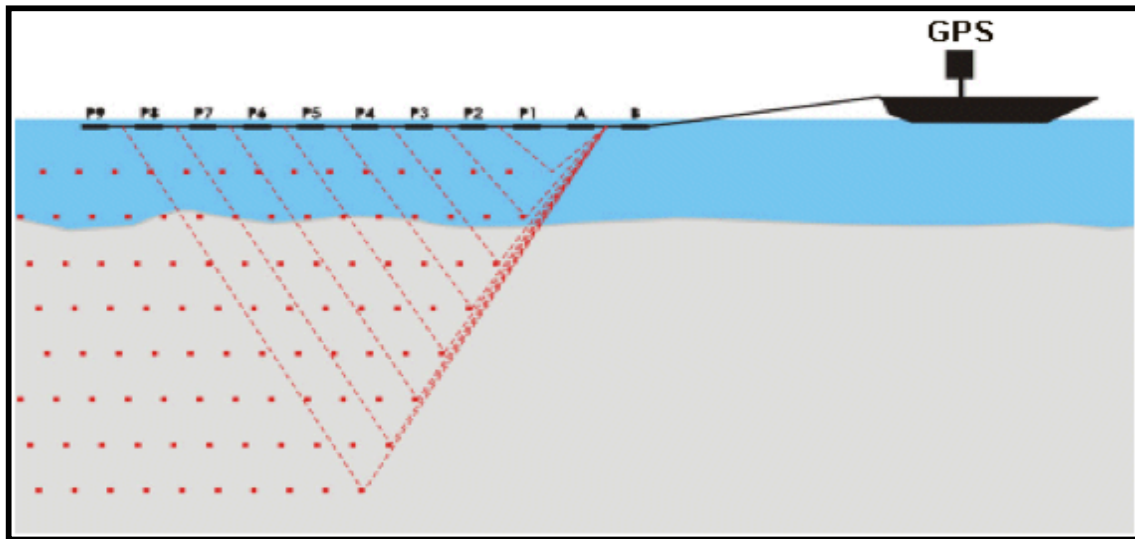


Figure 3. Image showing the continuous recording and storing of data from a GPS receiver using the SuperSting Marine. The SuperSting Marine continuously records and stores data from a GPS receiver. Current is injected every 3 seconds and 8 apparent resistivity values representing 8 depth levels are read for each current injection. Depth of penetration depends on length of the cable and array type (typically approximately 20% of the electrode spread length) (Advanced Geosciences, Inc.).

More recent developments enable the use of resistivity images collected as time-lapse stationary surveys over a desired timescale (i.e., tidal cycles) to estimate SGD rates. Preliminary CRPs surveys and time-lapse images (electrical resistivity tomography – ERT) are conducted with the +-resistivity cable deployed along the bottom of the bay. During the time-lapse imaging systematic measurements are taken to capture the changes in the subsurface porewater salinity/conductivity and estimate discharge over an 8-10 hour-period. In conjunction with time-

lapse images, continuous monitoring of radon (^{222}Rn) in water and air was conducted using *Durridge RAD7* monitors. Field parameters were monitored using an *Insitu Troll 9500*, to further constrain any potential SGD. Collected resistivity data was inverted and statistically evaluated using the *2D AGI EarthImager* software.

The AGI SuperSting R8 Marine is an 8-channel resistivity profiler that utilizes various electrode arrays, graphite electrodes, and EarthImager software, which allows the profiler to be used on land, towed on the waters surface and deployed on the bottom of the bay. The imaging system is paired with a 112 m cable with 56 electrodes spaced 2 meters apart with the ability to accurately image to a depth of approximately 20% the length of the cable. Resistivity readings of the area surveyed are collected through a dipole-dipole system that injects direct current through two current producing electrodes and measures the difference in voltage received by two potential electrode pairs (Advanced Geosciences, Inc.). The ability of the SuperSting R8 marine to take up to eight readings from each spaced electrode (2, 4, 6, 8) pair allows for in depth error correction and thus increasing the accuracy of the inverted image. For marine surveys the electrode cable is towed behind a boat along the desired transect (Figure 3). Transect beginning and end coordinates are entered into a Lowrance GPS for accurate geographic reference. When collecting marine resistivity data, it is crucial that the cable is pulled in the straightest path possible. Deviations from this path can add error to the readings.

The time-lapse ERT images are processed in Earth Imager using the time-difference inversion option, which creates an image showing subsurface areas with changes in porewater resistivity over time (expressed as % change in resistivity/conductivity). The plumes identified in these areas are used to calculate groundwater and contaminant mass fluxes to surface waters (Dimova *et al.*, 2012). A dipole-dipole configuration, which uses two current electrodes (C_1 and C_2) and

potential electrodes (P_1 and P_2) in close pairs that form a current and potential dipole, were employed in this study for data collection and processing (Loke, 2011; Dimova et al., 2012). Time-lapse surveys are conducted over a desired timescale. Most commonly tidal cycles are used in time-lapse inversions. Tide-induced SGD is relatively simple in theory, being that seawater enters the sea-land interface during rising and high tides and leaves the interface during low tides (Li and Jiao., 2013).

Porewater specific conductivity values collected in-situ are used to constrain the results from the inverted images to decrease the error associated with the estimation of groundwater discharge rates. Given the conductive nature of the imaged sediments and porewaters, and the expected constant resistivity of subsurface sediments (i.e. unconsolidated clays to silty-sands at depth below the nepheloid layer), we believe that the local resistivity contrasts are due to changes in porewater chemistry, thus resulting noise levels are negligible and will not affect the resolution of the resulting ER tomography (Friedel, 2003).

2.2.2. Salinity Mass Balance and Submarine Groundwater Discharge Flux Calculations

Time-difference inversion algorithms were used to calculate the percent difference in resistivity between six consecutive images collected over an eight-hour period during July and November/December field expeditions. Through this process the image collected at $t=1$ (the initial image) is used as the base/reference image from which the image collected at $t=2$ is subtracted and normalized. Furthermore, the image collected at $t=2$ is used as the base image from which the image collected at $t=3$ is subtracted and normalized and so on. In this matter, changes in the subsurface bulk resistivity can be monitored between each time-step. The overall resulting difference-image reveals changes in bulk resistivity over the entire monitoring period which is assumed to be caused by variations in pore fluid chemistry while the matrix properties

remain constant (Nyquist *et al.*, 2008). Groundwater plumes were identified and separated into boxed zones for each time-difference inversion image and the volume (V) of each zone was estimated using a 2-meter horizontal distance (Dimova *et al.*, 2012; Bighash and Murgulet, 2015). The defined zones for each image were superimposed onto the original ER images corresponding to the collection time and location in order to derive the corresponding salinities for mass-balance development. Plumes/boxed areas assumed to represent changes in salinity due to conductive groundwater flow were selected based on % changes exceeding the root mean square (RMS) of each time-difference image. Porewater salinities within these zones were corrected using the relationship between formation factor (F) and sediment porosity (ϕ) using equation 1 given by Archie's law (Archie, 1942). Based on sediment core description and well logs developed in the formation extending under the Corpus Christy Bay and the Upper Laguna Madre, we assume a clay-content of approximately 25%. Clay corrected Archie's constants have been derived using a least-squares fitting of log-porosity and log-resistivity values (Lee and Collett, 2006). The cementation exponent (m), is how the pore network increases the resistivity and is expressed in a range from 1.7-4.1, where increased permeability of the subsurface results in a decrease of the cementation exponent (Archie, 1942). The tortuosity factor (a) is used to account for variations in compaction, pore structure, and grain size in relation to flow path length and structure, and values lie between 0.5 and 1.5 (Archie, 1942). The clay corrected constants that assume a 25% clay content yield " m " and " a " values of 1.89 and 1.03, respectively. The porewater resistivity (R_p , Ωm) is then calculated using Archie's law for fully saturated media as expressed in equation 2. Salinity values for each superimposed zone were then estimated using equation (3) which allows for the conversion of ER-derived resistivity (R_p , Ωm) to salinity (S, parts per thousand (ppt)) (Manheim *et al.*, 2004):

$$F = a * \phi^{-m} \quad (1)$$

$$F = R_f/R_p \quad (2)$$

$$S = 7.042 \times R_p^{-1.0233} \quad (3)$$

Average porewater salinities were derived for the beginning/base (S1) and end/monitoring (S2) of each time-lapse survey. With this information, the volume of groundwater discharge was calculated using a salinity mass balance approach as described in equation 4.

$$V_{gwd} = V_{sal} * [(S1-S2)/S2] \quad (4)$$

In the above mass balance approach, the principle of conservation of both mass and salt is applied. Assuming a steady-state condition over a specified time, the SGD rate is calculated as the difference between the salinity inputs and outputs, not accounting for saltwater dispersion (or diffusion). Mass balances for each box are determined using the following criteria: fluxes into (out of) a box are positive (negative). This method also assumes that the process driving the change in salinity within the box is achieved through mass displacement, which replaces the pore fluid with groundwater of a different salinity mass, and that the rate of displacement is slow enough to be captured by each time-step. Furthermore, this method is based on the assumption that the entire volume of groundwater plumes, fresh or saline, will eventually discharge into surface waters under hydrologic conditions favoring groundwater discharge to surface water (i.e. upward hydraulic gradients). For a detailed description of this method, please refer to [Dimova *et al.* \(2011; 2012\)](#).

2.3. Radon Submarine Groundwater Flux Calculations

Radon is enriched in groundwater when compared to surface waters (typically 1000-fold or

greater). Because of its unreactive nature and short half-life ^{222}Rn is an excellent tracer to identify areas of significant groundwater discharge or sediment fluxes (Burnett and Dulaiova, 2003). Several studies demonstrate that continuous radon measurements could provide reasonably high-resolution data to evaluate changes of radon concentration of surface water at one location over time (Burnett *et al.*, 2001b; Burnett and Dulaiova, 2003). Continuous measurements of ^{222}Rn were conducted at 3 selected locations where time-lapse ER profiles were also acquired. The automated radon system (RAD 7 and the RAD AQUA accessories, Figure 4) was placed at the end of each resistivity transect on the deck of the research vessel.

The monitoring system measures ^{222}Rn from a constant stream of water (driven by a peristaltic pump) passing through an air-water exchanger. The exchanger distributes radon from a running flow of water to a closed air loop that feeds to the RAD 7 radon-in-air monitor. A detailed description of RAD 7 capabilities and measurement principles can be found in Burnett and Dulaiova (2003). Radon measurements were integrated over 45 minute intervals at a depth of 0.5 m above the bottom of the bay and remained stationary by an anchored 15 pound weight.

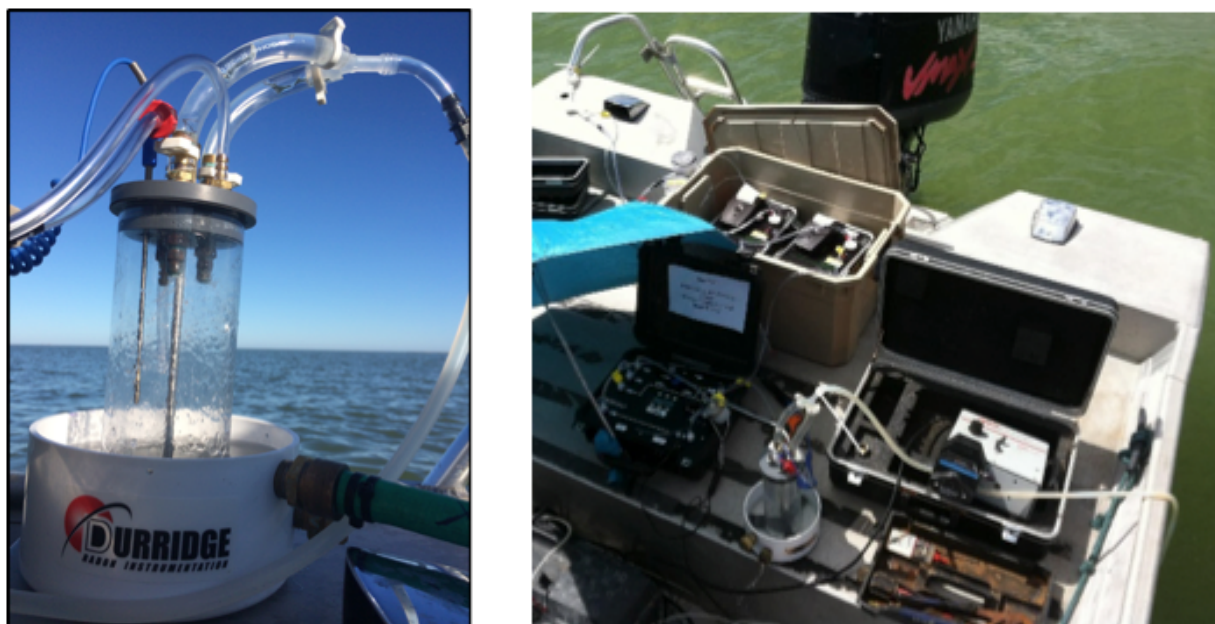


Figure 4. Automated radon system (RAD 7) and the RAD AQUA accessories used to measure

continuous radon in water and air.

The main principle behind using continuous radon measurements to quantify groundwater discharge rates to surface waters is based on the inventory of ^{222}Rn over time accounting for losses due to mixing with waters of different radon concentrations (i.e. low concentrations offshore waters), atmospheric evasion, and sediment-supported fluxes (Figure 5). Thus, concentrations over time, if exceeding the sediment-supported, are believed to result from groundwater and can be converted to radon fluxes (Burnett and Dulaiova, 2003).

The atmospheric loss of Rn was estimated using the equations presented by Macintyre *et al.* (1995) that calculate the gas exchange across water-air interface using the radon concentration gradient, temperature and wind speed.

Radon mass balance is:

$$F_{\text{total}} = F_{\text{sed}} + F_{\text{offshore}} - F_{\text{atm}} - F_{\text{nearshore}} - F_{\text{mix}} - \lambda Rn \quad (5)$$

The terms are estimated according to:

$$Ex \text{ } ^{222}\text{Rn} = ^{222}\text{Rn}_{\text{total}} - ^{226}\text{Ra} \quad (6)$$

$$I_{\text{Rn}} = Ex \text{ } ^{222}\text{Rn} * \text{water depth} \quad (7)$$

Used to estimate excess ^{222}Rn inventories (I_{Rn}).

$$\text{Ebb Tidal Height Correction} = ^{222}\text{Rn}_{\text{nearshore}} * \Delta\text{tidal height} \quad (8)$$

$$\text{Flood Tidal Height Correction} = ^{222}\text{Rn}_{\text{offshore}} * \Delta\text{tidal height} \quad (9)$$

$$\text{Normalized } I_{\text{Rn}} = I_{\text{Rn}} - \text{Tidal Height Correction} \quad (10)$$

NOAA tidal data was used to normalize tidal conditions. Over the span of sampling, changes in tidal height though negligible, were taken into account in the radon mass balance equations.

$$F_{\text{atm}} = k(C_w - \alpha C_{\text{air}}) \quad (11)$$

Where F_{atm} = degassing to the atmosphere ($\text{Bq/m}^2 \cdot \text{d}$), $k=k_{(600)}$ radon transfer velocity (m/s , m/d , cm/hr), C_w =concentration of Rn in water (Bq/m^3), α =Ostwald coefficient, partition coefficient of Rn between water and air (dimensionless), and C_{air} =concentration of Rn in air (Bq/m^3).

$$F_{\text{sed}} = (\lambda_{\text{Rn}} * D_s)^{1/2} * (C_{\text{eq}} - C_o) \quad (12)$$

Where F_{sed} =flux of radon from the sediment ($\text{Bq/m}^2 \cdot \text{d}$) is determined using, λ_{Rn} =decay constant of radon (d^{-1}), D_s =the effective wet bulk sediment diffusion coefficient in sediments (m^2/min), C_{eq} =is the radon released by radium in the sediments during sediment equilibration experiments (Bq/m^3), and C_o =is the radon in the overlying water at the sediment-water interface multiplied by the sediment porosity to obtain a value corresponding to the ^{222}Rn concentration in wet sediment (Bq/m^3).

$$F_{\text{net}} = \Delta I^* / \Delta t(\text{s}) \quad (13)$$

Net radon fluxes were estimated using, I^* =as the inventory corrected for supported ^{222}Rn (^{226}Ra), changes in water level, atmosphere evasion, and sediment supported (Bq/m^2) and t =time interval during sampling (1 hour).

$$F_{\text{mix}} = \text{maximum } [-] F_{\text{net}} \quad (14)$$

$$F_{\text{total}} = F_{\text{net}} + F_{\text{mix}} \quad (16)$$

Fluxes of radon could not be measured for longer than eight hours for each of the seasonal time-lapse sampling events because of adverse weather conditions (e.g., at winds of more than 19 kilometers per hour (kph) bay conditions become very difficult for sampling and data collection). Consequently, the effect of tides could not be fully addressed using the presented methods. Nevertheless, changes in water levels of no more than 0.3 m are recorded in this area due to tidal

fluctuations (NOAA, 2014). It is assumed that the lower radon fluxes observed during the monitoring time are due to mixing with offshore waters of lower concentration.

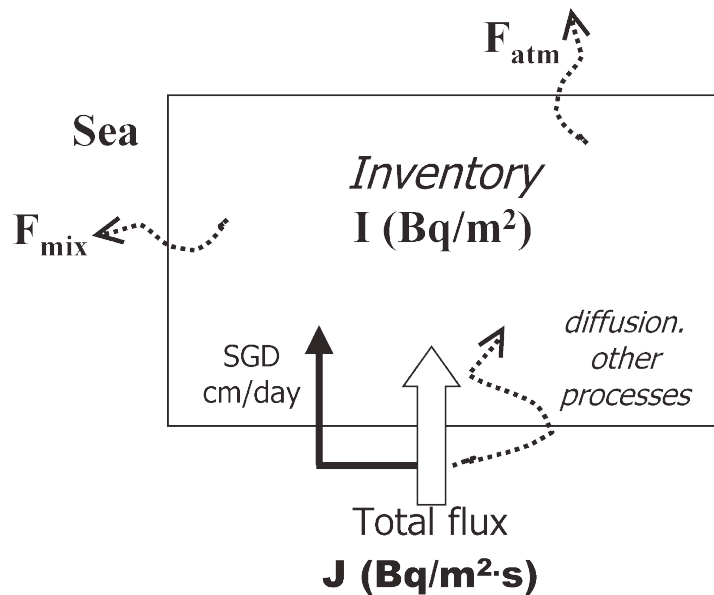


Figure 5. Conceptual model showing the radon inventory per unit area for estimating groundwater discharge (Burnett and Dulaiova, 2003).

The maximum absolute values of the observed negative fluxes during each time-series event at each location are used to correct radon fluxes for losses via mixing (Dulaiova *et al.*, 2006). The estimated losses due to atmospheric evasion and mixing with low radon offshore waters are added to the net fluxes resulting in a total radon flux used to calculate SGD rates calculated using equations presented by Burnett and Dulaiova (2003). Furthermore, sediment fluxes were calculated using laboratory equilibration experiments from sediment cores collected at each time station using the following equation (17) presented by Corbet *et al.* (2000). Finally, water fluxes were calculated using the time series data and equation 17 derived by Burnett and Dulaiova (2003). It is the attempt of this study to conservatively estimate such fluxes and rates by taking into account a large variety of losses (wind, tide, mixing, etc.), and thus helping to legitimize the importance of SGD to the overall budget.

$$q(\text{m/s}) = F_{\text{total}} / E \times 222 R_{\text{ngw}} \quad (17)$$

Where q (cm/day) is calculated by dividing the total estimated ^{222}Rn fluxes (T_{total} , $\text{Bq/m}^2\cdot\text{s}$) by the concentration of excess ^{222}Rn ($\text{Ex } ^{222}\text{Rn}_{\text{gw}}$, Bq/m^3) in the fluids entering the system (i.e. equation [Burnett and Dulaiova \(2003\)](#)).

2.4. Nutrient and Chlorophyll-a Sampling

Nutrient samples were collected from porewater and water column in acid-washed polycarbonate bottles and stored on ice for the duration of the sampling expedition. Chlorophyll-*a* analyses were run on samples collected from the water column at different depth, depending upon depth to sediment-water interface. Chlorophyll- α was determined from samples collected on, and extracted from Whatman GF/F filters (nominal pore size $0.7 \mu\text{m}$). Chlorophyll was extracted using 90% acetone and analyzed fluorometrically. Inorganic nutrients (nitrate + nitrite (N+N), nitrite, silicate, orthophosphate, ammonium) were determined in the filtrate of water that passed through GF/F filters using a Seal QuAAtro autoanalyzer. DOC and TDN were determined in the filtrate of water that passed through GF/F filters using a Shimadzu total organic carbon analyzer (TOC-V) with nitrogen module. Dissolved organic nitrogen was estimated as the difference between TDN and inorganic nitrogen.

3. Results and Discussion

3.1. Continuous Resistivity Profiles

Preliminary continuous resistivity profiles were collected along each of the five transects. These CRP images (Figures 6-10) were used to aid in the selection of sampling sites, with potential SGD, for both seasonal and time-lapse sampling. Transect 1 (Figure 6) was collected within the Upper Laguna Madre and showed minimal signs of SGD near shore and small pockets further offshore. The near shore plumes of higher resistivity hint towards a possible sandy pocket of

freshwater upwelling from aquifer formations below the predominantly clay subsurface typical of the intracoastal water way. The saltier plumes within the shallower portions of the subsurface are likely sinking into these deeper layers, this could be caused by density-driven free convection processes that enhance upwelling of fresher/brackish water and discharge to the surface water. This is explained in more detail by Bighash and Murgulet (2015) and Stevens et al. (2009), which showed that such processes are common in the Laguna Madre and Oso Bay.

The second transect (Figure 7) was collected at the mouth of Oso Bay and out into Corpus Christi Bay. In the shallower portion of the image, there are signs of significant interaction between SGD and surface waters. This interaction could be the results of anthropogenic activities, such as dredged channels to allow boats to pass under the bridge disrupting the predominate clay layers and allowing for sandy conduits. Together with extensive construction and development, these activities likely disrupted the less conductive layer in the subsurface and thus allowed for such interactions. The third transect (Figure 8) extended from the mouth of the Laguna Madre out into Corpus Christi Bay. Similar to the Oso-Corpus Christi Bays transect, the likely presence of a disrupted impermeable layer which allow for mixing of saltwater with brackish water. These observed anomalies indicate that some of the interchanging plumes are of much lower resistance than surface water, which would indicate that groundwater could be a source of salts locally to the bay.

The fourth transect (Figure 9) spanning from North Padre Island's west coastline, northwest reaching close to Shamrock Island, showed that SGD interaction may occur at multiple locations. This portion of the bay and island is relatively underdeveloped, characterized by fewer disruptions in the subsurface. In contrast to the majority of the bay, near the island there was a large sandy surface and shallow layer. This resulted in the majority of the interaction zones

associating with the nearshore portion of the transect and fading with distance offshore into Corpus Christi Bay where the presence of a more conductive (less permeable or hydrologically conductive) layer similar to the second and third transects is visible. Transect 5 (Figure 10) was collected off of University beach and progressed further offshore into the bay. There is a very minute sign of SGD interaction near shore but beyond this point the less permeable layer is very prevalent and there are no signs of SGD interaction.

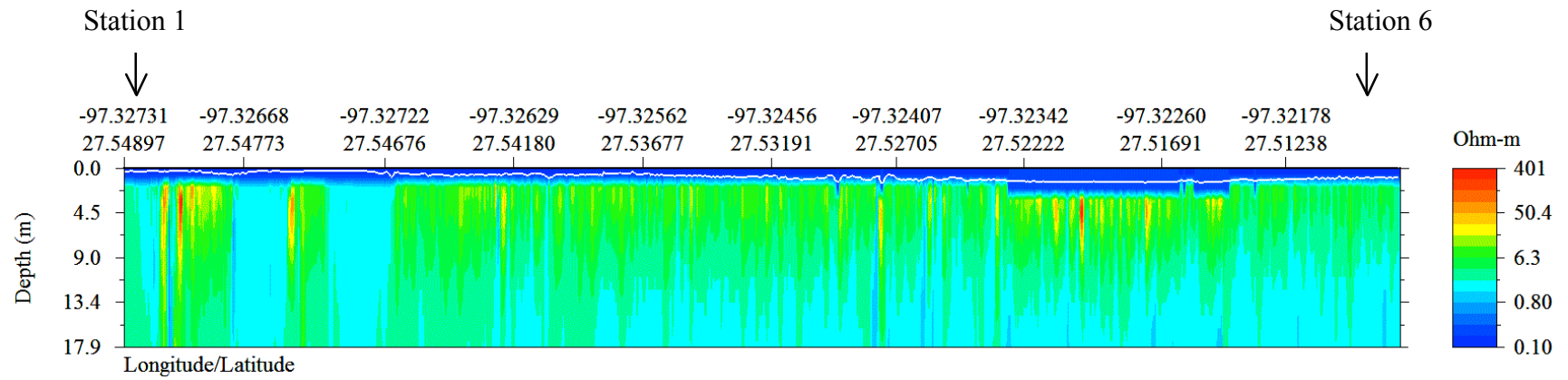


Figure 6: Continuous resistivity profile for the Laguna Madre transect (T1).

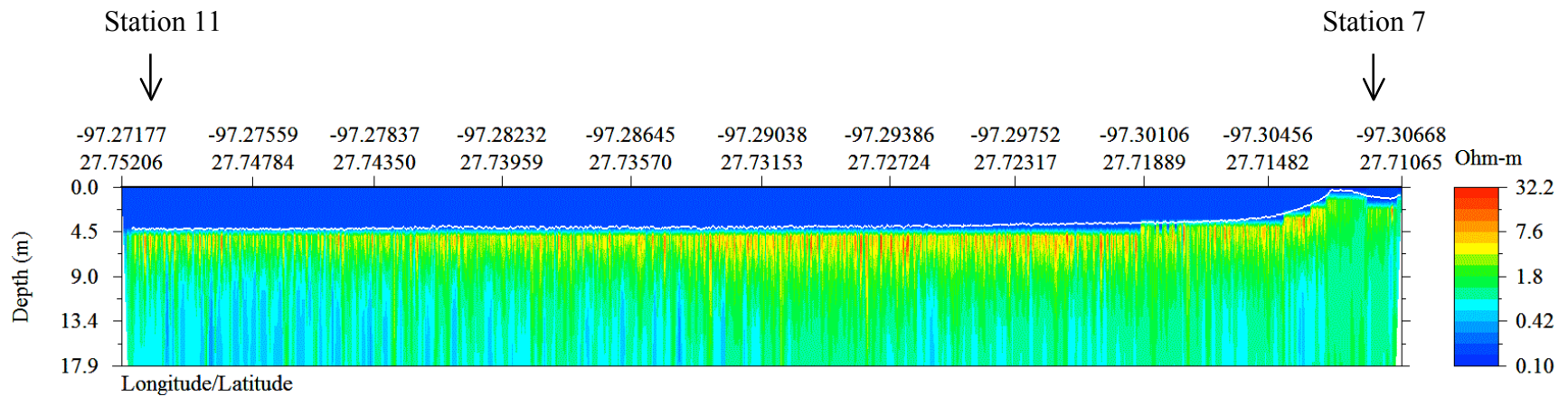


Figure 7: Continuous resistivity profile for the Oso Inlet transect (T2).

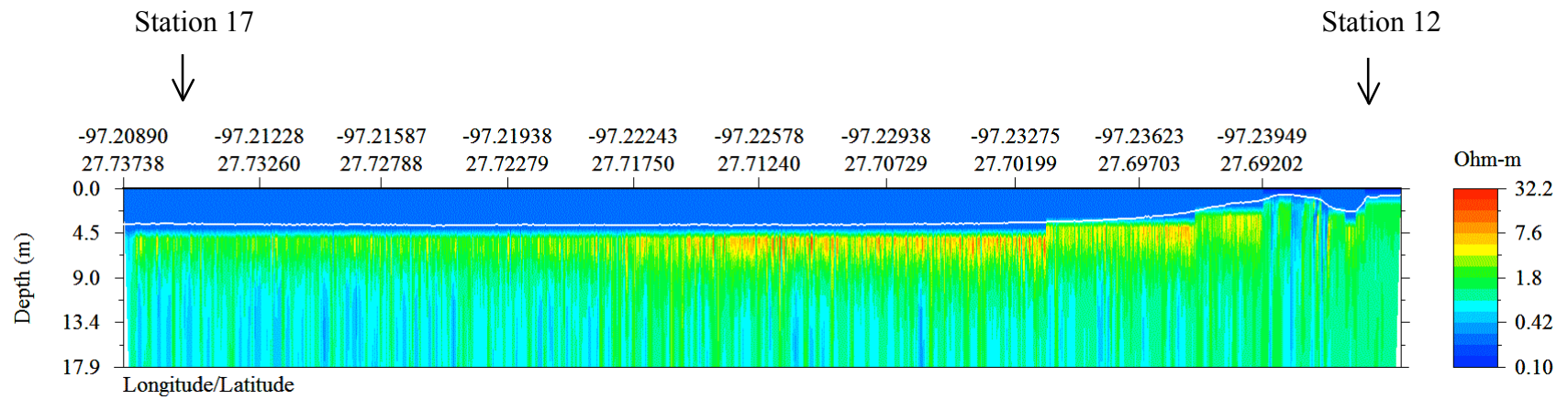


Figure 8: Continuous resistivity profile for the Laguna Madre Mouth transect (T3).

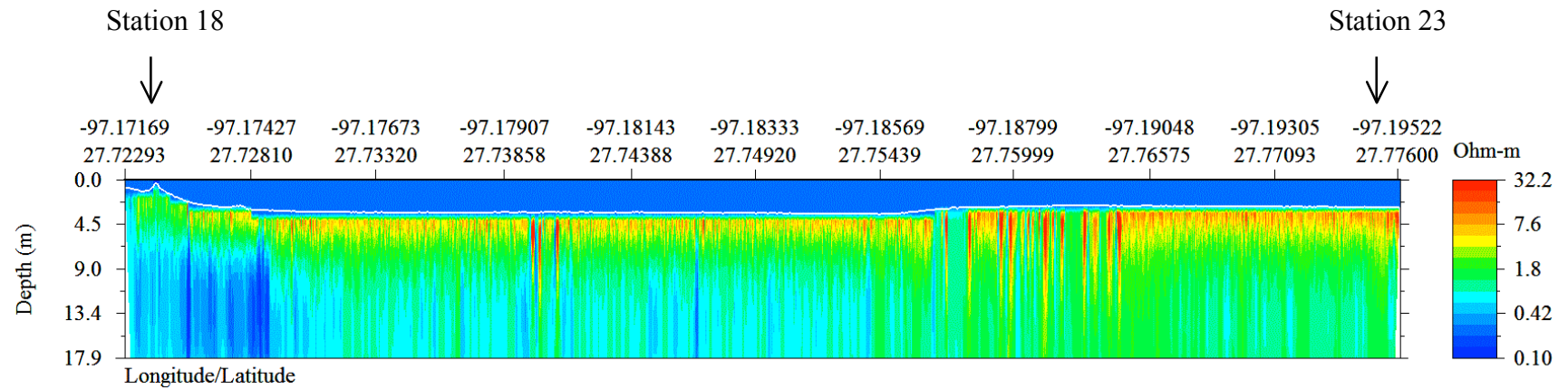


Figure 9: Continuous resistivity profile for the Shamrock Island transect (T4).

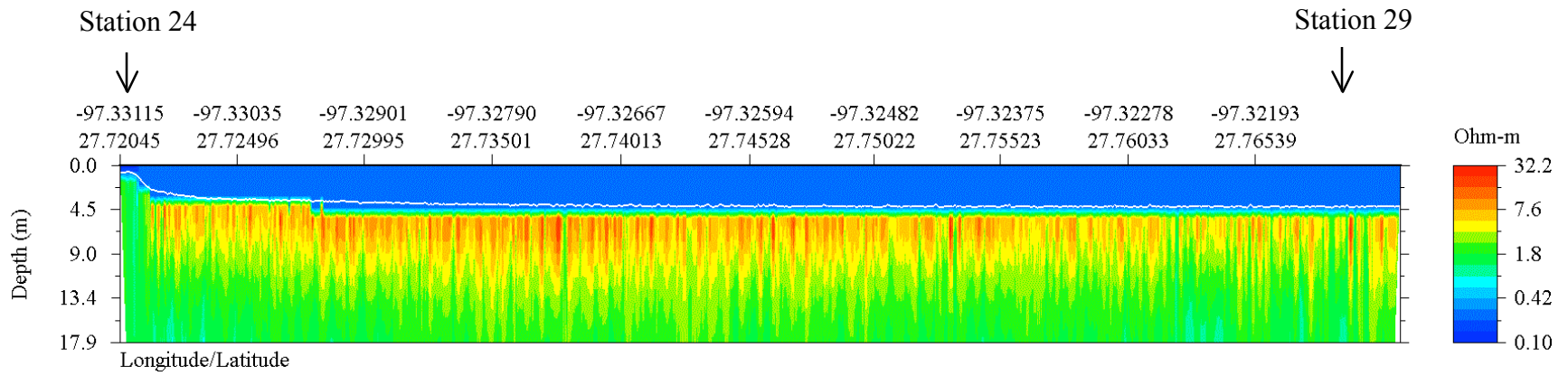


Figure 10: Continuous resistivity profile for the University Beach transect (T5).

3.2. Time-Lapse Resistivity Profiling and Resistivity-Derived SGD Rates

Time-lapse ERT imaging was collected at one location for transects 2, 3, and 4 (signified by stars in Figure 1), that were found to show groundwater-surface water interaction from the preliminary CRP images. Time-lapse profiles or ERTs were collected over a 5-7 hour span at a stationary location in July (summer) 2014 and again in November-December (fall) 2014 to capture any seasonal variances associated with precipitation events. Represented in Figure 11, the summer and fall sampling events captured the seasonal rainfall highs and lows for the year. The range of resistivity values was very narrow (0.10-1.4 Ωm). Changes in resistivity are displayed on a color spectrum scale from red to deep blue (red being an increase in resistivity, blue being a decrease, and green representing little to no change or zero).

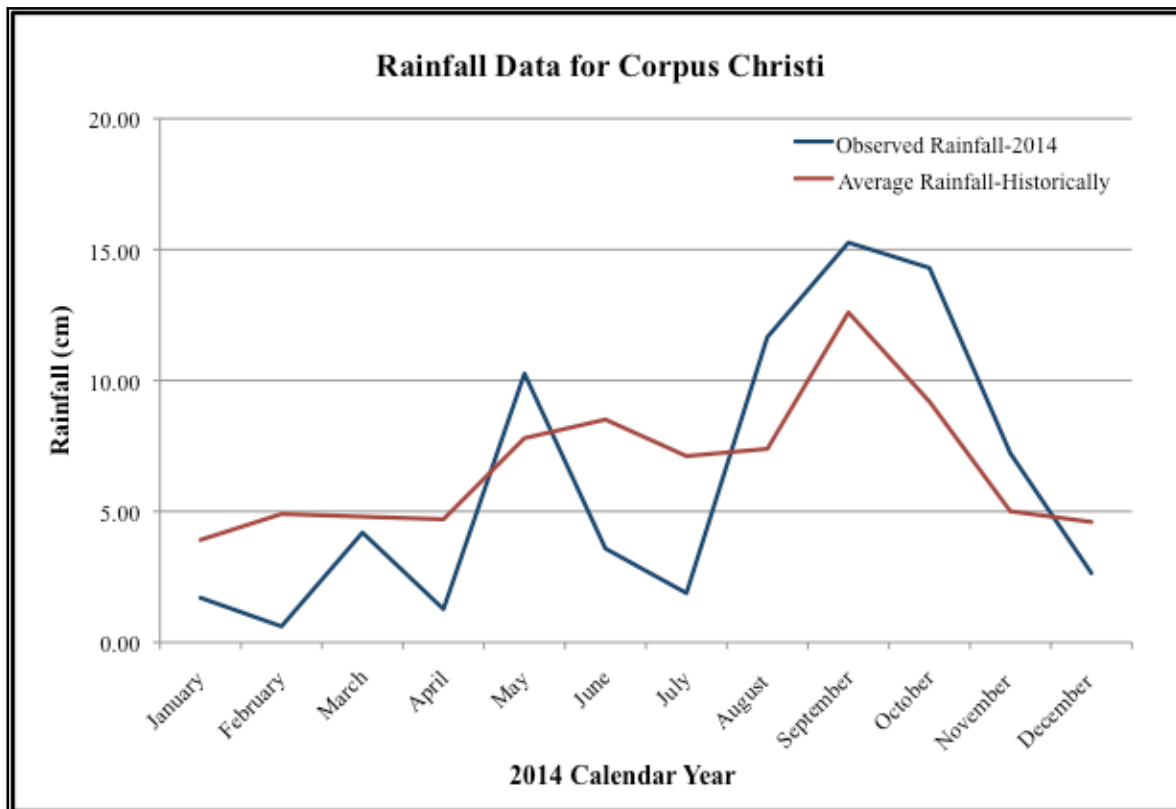


Figure 11: Rainfall data for the 2014 calendar year compared to historical averages (NOAA, 2014).

The time-lapse ER images for each location showed a varied degree of groundwater-surface water interaction for both summer and fall. Plume location and extent of change were variable among the two seasons, but result in relatively similar estimated SGD rates. For example, the Oso Inlet location (Figures 12-13), in summer, shows a large interaction between the water column and the first 3-5 m of subsurface along the majority of the 112 m (represented in the images as 0-108) span and shows a decrease in salinity. On the other hand in fall, the images showed large plumes of saline water, less uniform shape and structure, and found deeper within the 26 m depth of the profile. Though the intensity of change in porewater chemistry and location of plumes changed, seasonally the SGD rates derived from the salinity mass balance show similar discharge rates for summer (7.4 cm/d) and fall (9.2 cm/d).

The Laguna Madre Mouth yielded the highest percent change in porewater chemistry when compared to the other locations (Figures 14-15). The summer time-lapse computed difference inversion showed a high range of percent change in resistivity (40%) among the various plumes. Fall had a smaller difference percentage (12%) but depicted a large plume of saline water along most of the transect, within the first 3-13 m. SGD rates were estimated to be 66.7 cm/d for summer. During fall, although a smaller percent change was measured, a larger area was impacted, resulting in a 74.1 cm/d discharge rate. Porewater collected from the Laguna Madre Mouth station shows an increase in salinity from summer to fall. Although the calculated SGD rates, using the salinity mass balance and radon-derived methods, vary to some degree, the difference in bulk resistivity supports the possibility of interaction between the subsurface interstitial fluids and water column via preferential flow conduits caused by small-scale heterogeneity.

The Shamrock Island inversions (Figures 16-17) generated consistent fresher water saturation within the top 0-5 m of the subsurface, which is consistent with field observations during porewater sampling revealing the existence of a sandy layer. These saturated plumes vary slightly from summer to fall, with the only difference being a large upwelling of saline water during the summer sampling near the 96 m of the transect at a rough depth of 5-10 m (Figure 16). The range of resistivity for the Shamrock Island transect is narrower than the other locations (0.14 to 0.72 Ωm) but the large and consistent change in porewater chemistry along the shallow portions of the transect yield a more consistent seasonal salt- mass-balance derived SGD rate. The summer and fall SGD rates are 13.5 and 10.3 cm/d., respectively.

Station 7 (Continuous ^{222}Rn monitoring)

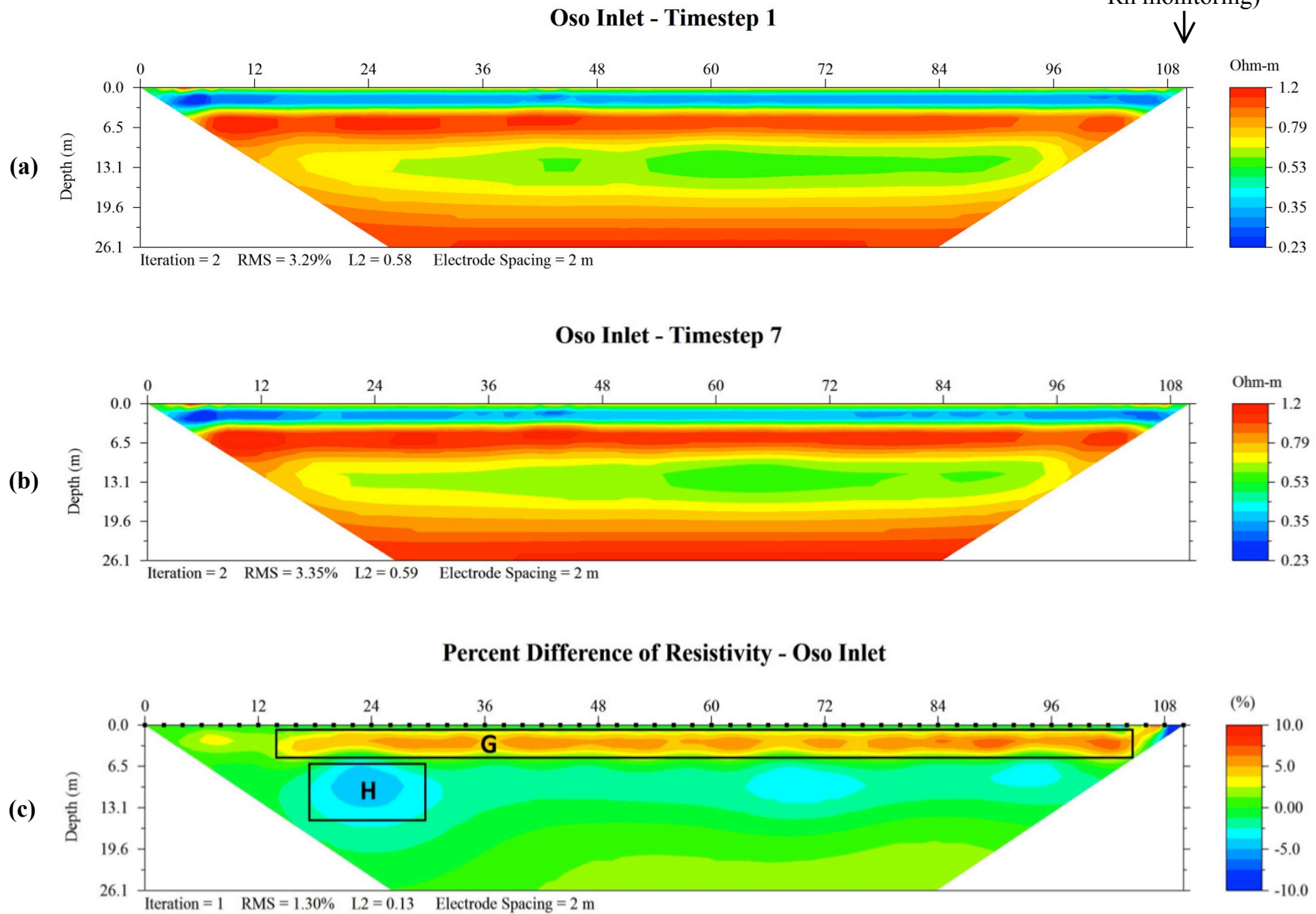


Figure 12: Summer time-lapse resistivity profiles for Oso Inlet, show the first (a) and last (b) inversions, and computed percent difference (c) in resistivity over a seven-hour period.

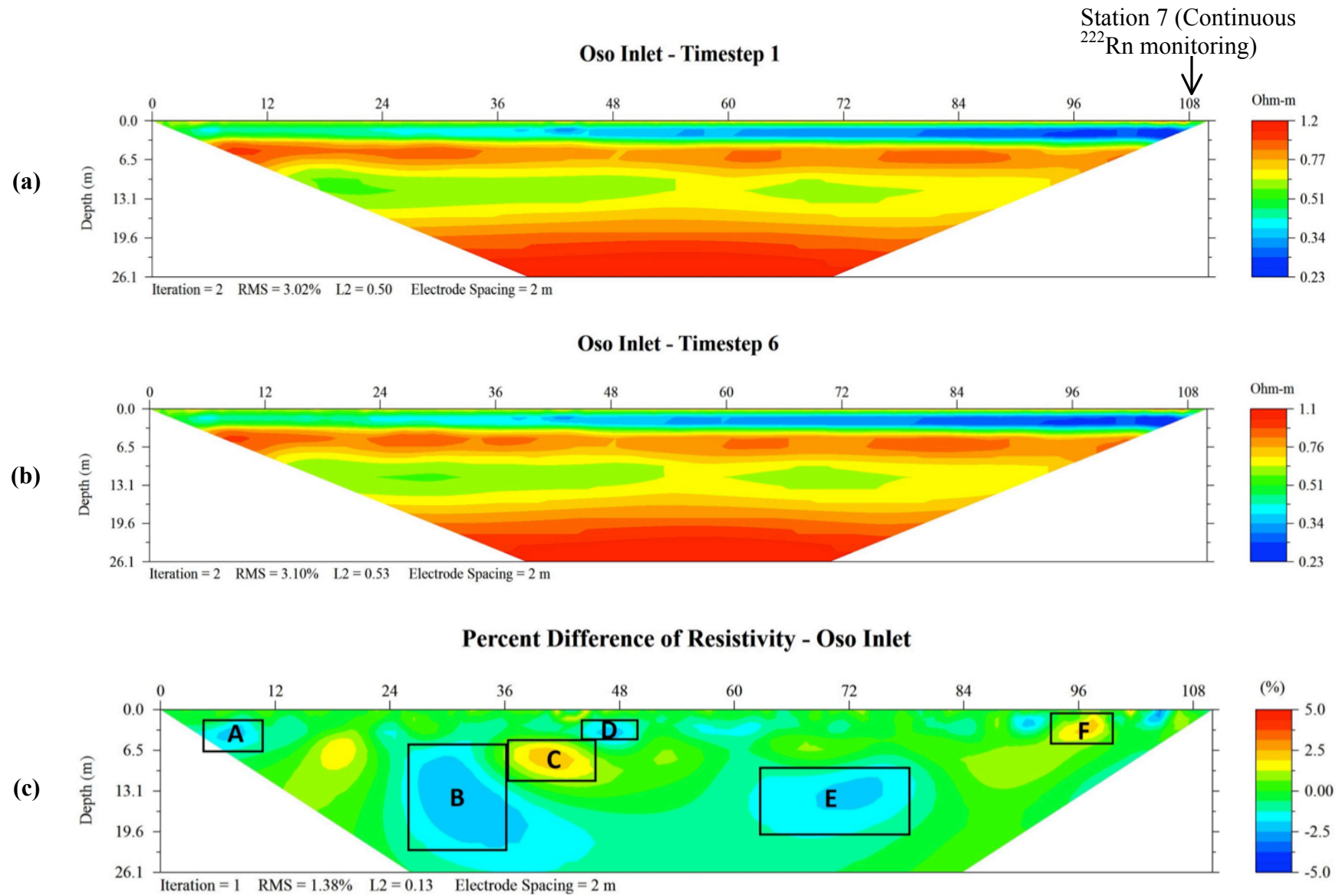


Figure 13: Fall time-lapse resistivity profiles for Oso Inlet, show the first (a) and last (b) inversions, and computed percent difference (c) in resistivity over a seven-hour period.

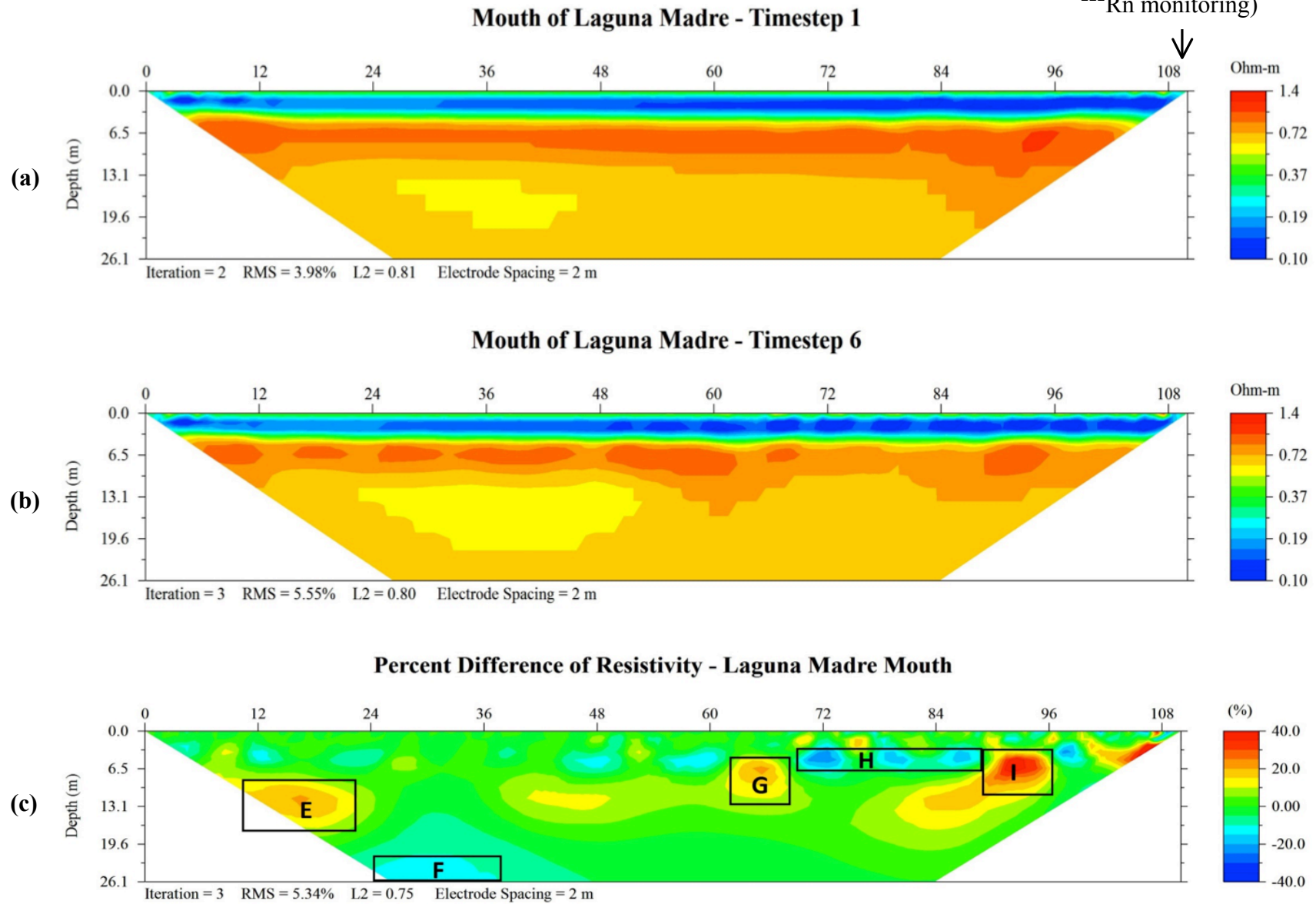


Figure 14: Summer time-lapse resistivity profiles for Laguna Madre Mouth, show the first (a) and last (b) inversions, and computed percent difference (c) in resistivity over a seven-hour period.

Station 12 (Continuous ^{222}Rn monitoring)

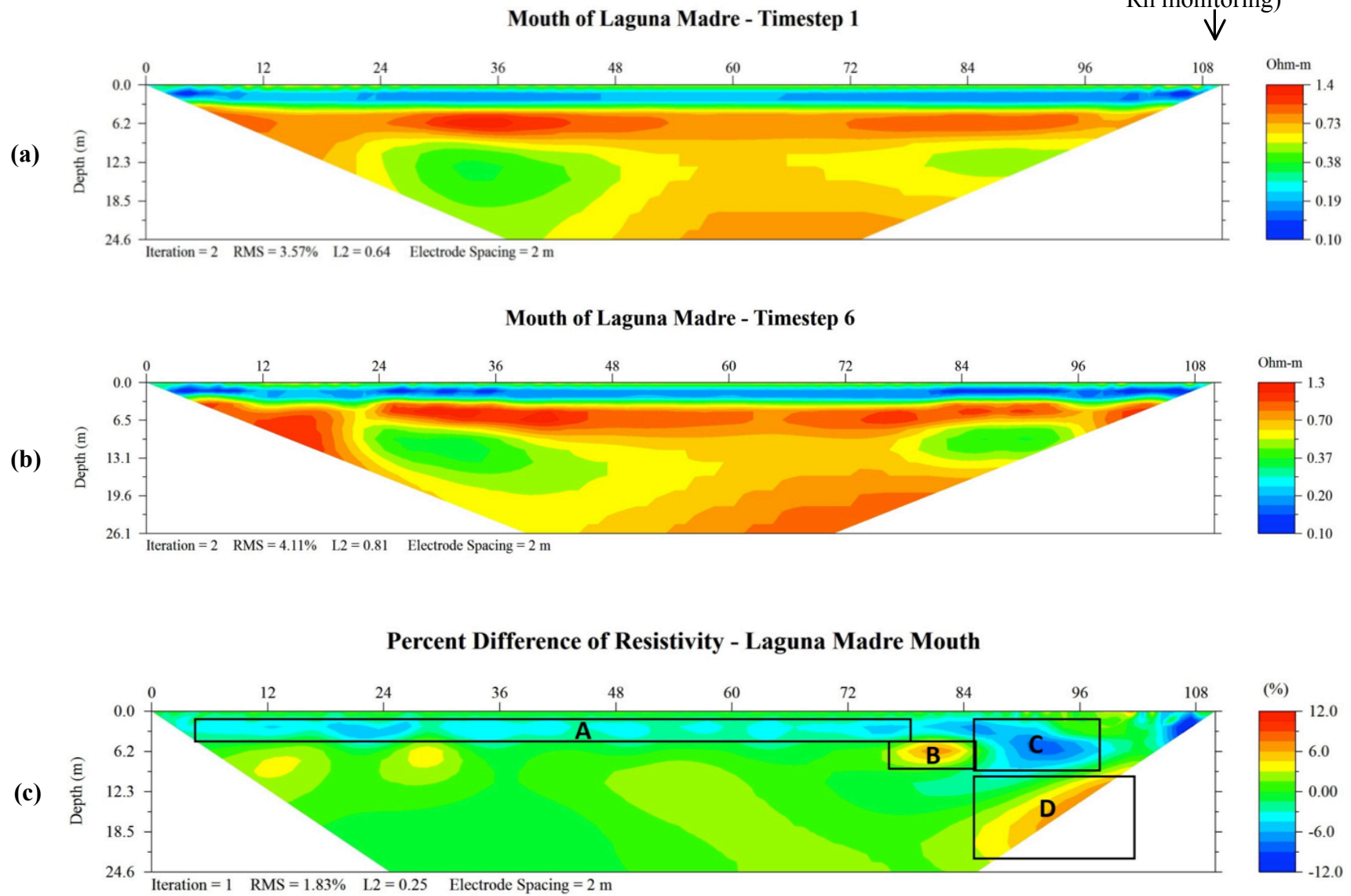


Figure 15: Fall time-lapse resistivity profiles for Laguna Madre Mouth, show the first (a) and last (b) inversions, and computed percent difference (c) in resistivity over a seven-hour period.

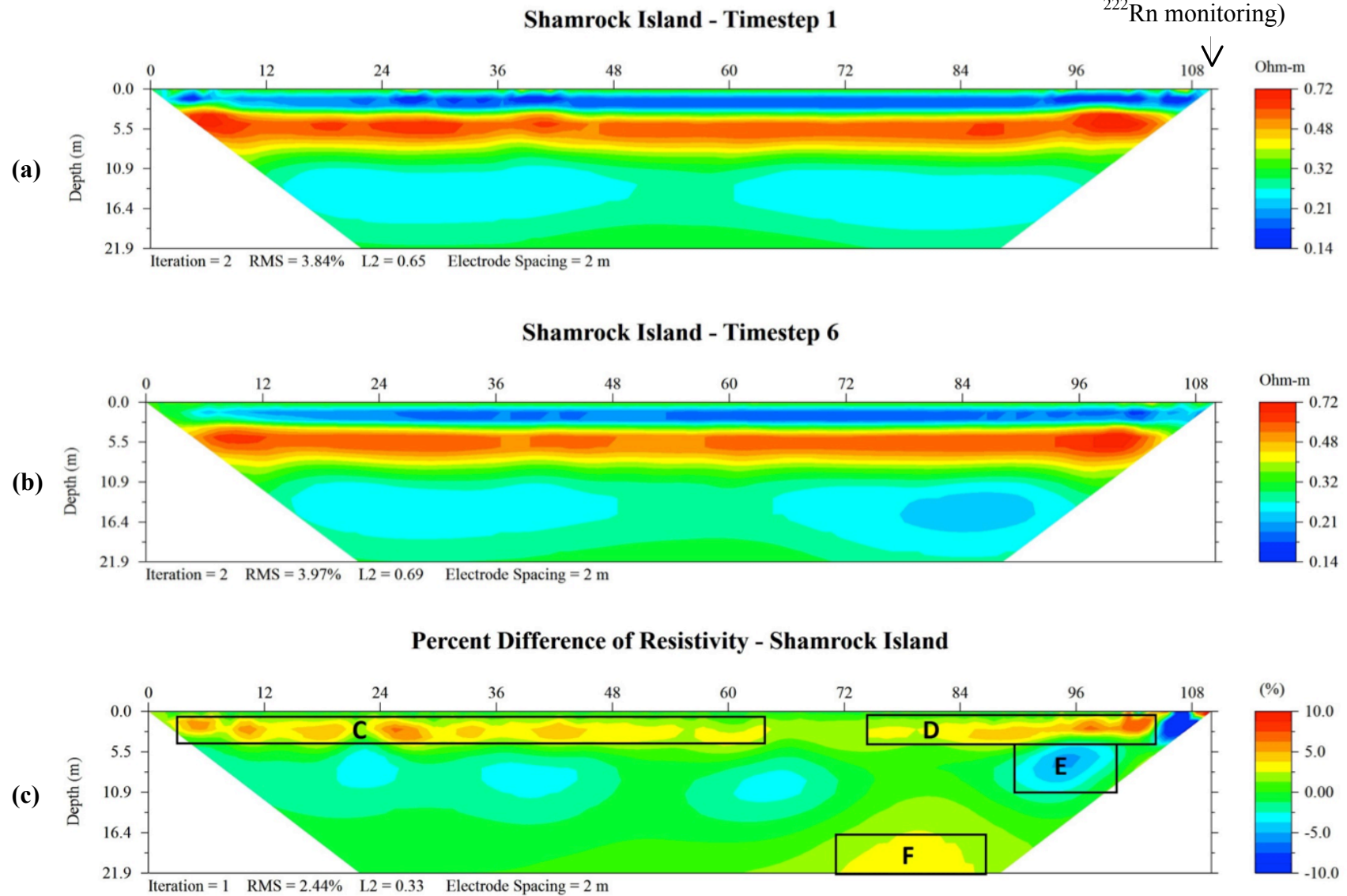


Figure 16: Summer time-lapse resistivity profiles for Shamrock Island, show the first (a) and last (b) inversions, and computed percent difference (c) in resistivity over a seven-hour period.

Station 18 (Continuous ^{222}Rn monitoring)

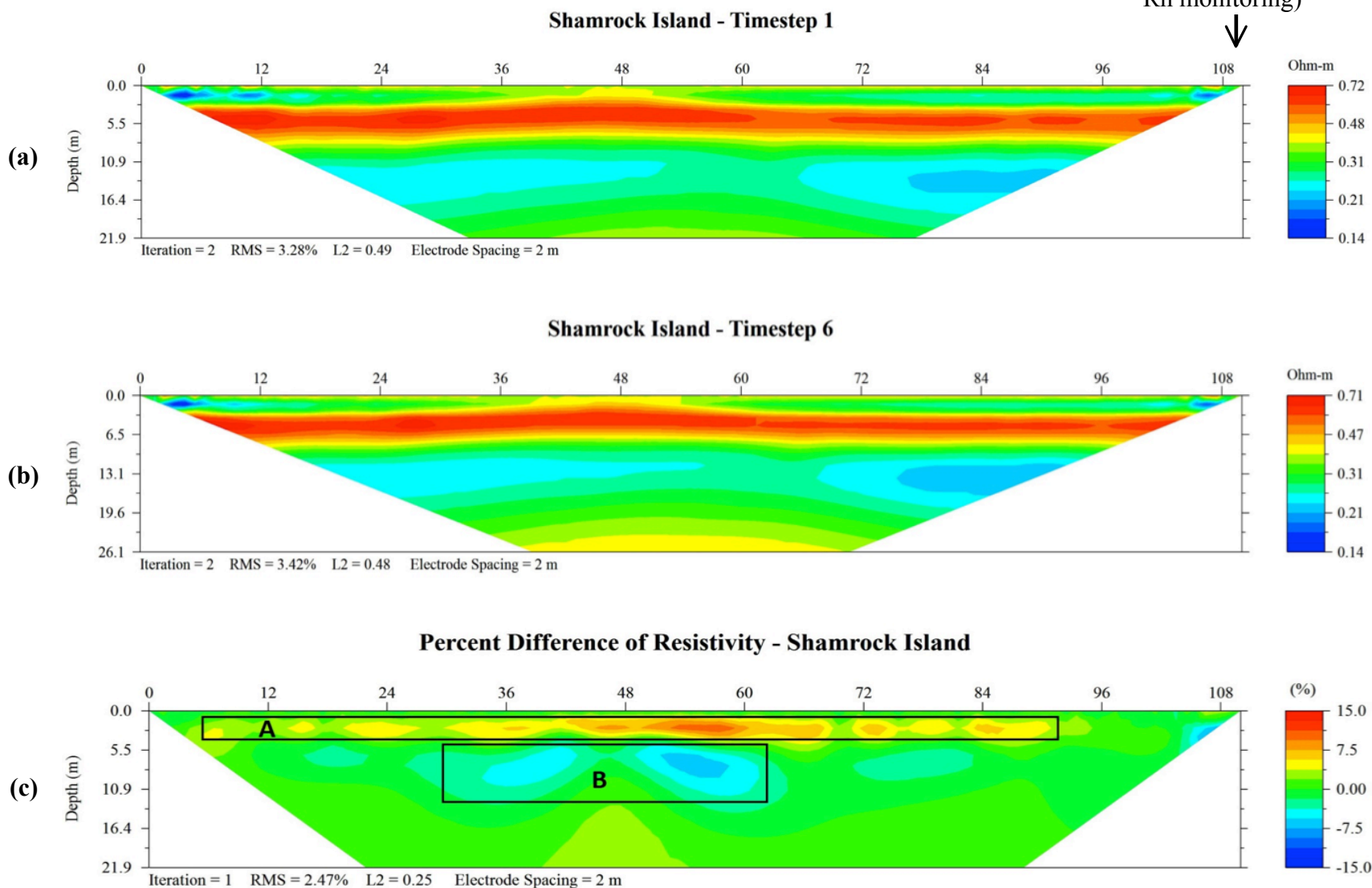


Figure 17: Fall time-lapse resistivity profiles for Shamrock Island, show the first (a) and last (b) inversions, and computed percent difference (c) in resistivity over a seven-hour period.

3.3. Radon-derived SGD Rates

Radon monitoring was conducted in parallel to time-lapse resistivity surveying at each location. The radon monitor and YSI multi-parameter probe (DO, Conductivity, and pH) were deployed off the deck of the boat near the closest electrode of the resistivity cable. Due to the smaller effective area of coverage, the RAD7 is able to sample (1 m²). When compared with the resistivity inversions (112 m²) it should be noted that the resulting SGD rates derived from the ²²²Rn do not take into account the hydrologic and hydrogeologic “heterogeneity.” Despite these limitations, the use of the two techniques to estimate SGD rates allows us to differentiate between fresh groundwater and recirculated seawater, delineate seepage faces as dependent of sediment heterogeneity and convective flow caused by density differences.

ER SGD monitoring only captures changes over the duration of a day (i.e. daylight), but a continuous record of ²²²Rn inventory and evaluation of SGD rates are provided at different locations and for two different seasons. South Texas experiences very mild tidal fluctuations (0.02-0.08 m observed tidal height fluctuations), thus it is expected that SGD rates would not be significantly affected by these changes that are usually captured over longer periods of time as depicted in similar studies (hours to days and months). The correlations between the ²²²Rn fluxes and tidal cycle are negligible, but there seems to be a fluctuation over the 8-hour period, which suggests the existence of other influences on groundwater discharge, such as wind speed and increased mixing.

The total estimated radon fluxes (Bq/m²s) were divided by the ²²²Rn activity of the advective fluids sampled from multiple wells surrounding the study area (5,149 Bq/m²) for each time interval (1 hour). The integrated water flux results were averaged for the 8-hour period and ranged from 33.7-280.2 cm/day (average = 119 ± 24.7 cm/d) in the summer and 12.5-374.1 cm/d

(average = 161 ± 35.0 cm/d) for the fall. Using the ER time-lapse spatial distribution of seepage faces and radon-derived seepage rate it was possible to create an estimated SGD rate across the 112-m transect per sampling site.

	Oso Inlet Summer	Oso Inlet Fall	Laguna Mouth Summer	Laguna Mouth Fall	Shamrock Island Summer	Shamrock Island Fall
222Rn flux on station (cm/d) 	280.2	374.1	43.2	12.5	33.7	96.5
ER flux on station (cm/d) 	21.0	53.0	46.0	27.0	15.0	21.0
222Rn SGD rates (m ³ /m.d) 	11.2	15.0	1.7	0.5	1.3	3.9
ER SGD rates (m ³ /m.d) 	0.8	2.1	1.8	1.1	0.6	0.8
Std Deviation (222Rn)	48.3	71.3	15.2	10.7	10.7	22.9
RMS Error (ER)	1.1	2.7	2.3	3.7	0.8	1.1

Table 1: Time-lapse ER and ²²²Rn-derived flux and SGD rates.

Volumetric discharge rates were obtained by normalizing SGD fluxes to a 2 m² (similar to the ERT-derived rates) ranged from 1.3-11.2 m³/m.d in summer and 0.5-15.0 m³/m.d in fall (Table 1). When compared with similar studies in various areas, these estimates (including the largest errors) are similar. For instance, Bokuniewicz et al. (2004) estimated SGD rates in Ubatuba, Brazil to vary between 0.07-15.2 m³/d (and a study performed in Nueces Bay Texas, estimated SGD rates are significantly larger ranging from 20×10^4 - 53×10^4 m³/d (Breier et al. 2004). Though Nueces Bay is located in close proximity to CCB, sediment variations, inputs, and overall geological locale and structure could possibly explain the exponentially larger SGD rate estimates.

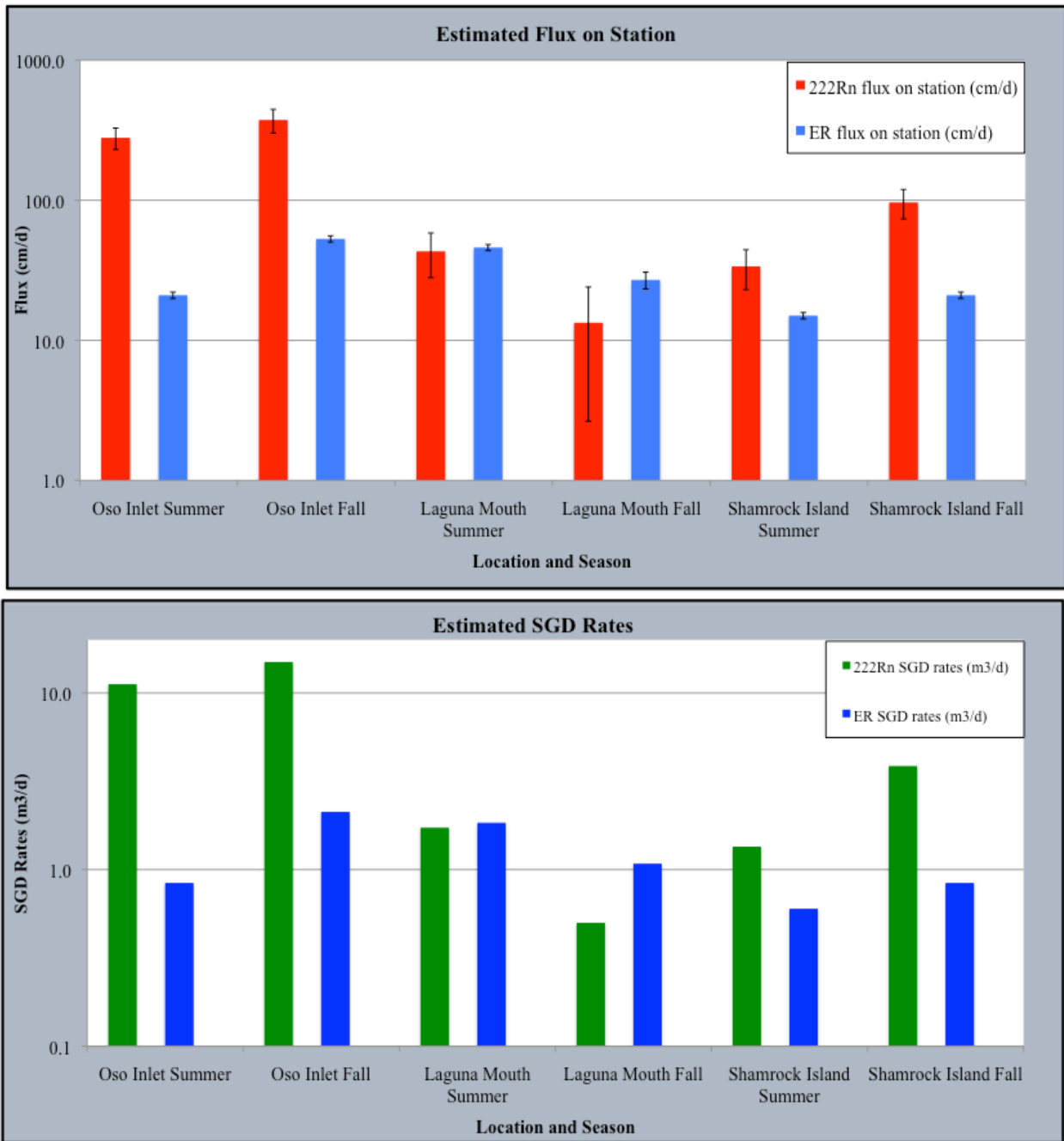


Figure 18: Chart (a) shows the estimated flux rates (^{222}Rn and ER on station and line) for each location and season. Chart (b) shows the estimated SGD rates (^{222}Rn and ER) for each location and season.

The radon-derived groundwater fluxes differ significantly when compared with the rates estimated using the ERT time-difference inversions (Table 1). For instance, radon-derived

fluxes were lower for the Laguna Mouth transect when compared to the resistivity SGD rates for both summer and fall, but the radon-based fluxes were larger by an order of magnitude in both the summer and fall seasons at the Oso Bay inlet location. Elevated radon-derived time-lapse estimates are likely the result of both groundwater and recirculation within the shallow portions of the bay bottom sediment. ERT inversions reveal potential groundwater movement not only in the shallow substrate but within the underlying shallow aquifer. These images also show that the flow and transport pathways are likely to vary with time, thus hinting at the heterogeneous nature of SGD likely as a result of changes in hydraulic gradients. Large variations in porewater ^{222}Rn concentrations were measured throughout CCB (174 to 21,547 Bq/m³). Changes in hydraulic gradients are expected in the Texas Gulf Coast, which is affected by droughts and extreme rain events (Sugita and Nakane, 2007). Direction and magnitude as well as source of groundwater flow could change significantly due to these changes (de Vries and Simmers, 2002).

Radon concentrations of the upwelling fluids are crucial in groundwater flux estimates determined using radon as the tracer. Changes in radon concentrations by one order of magnitude will result in an increase or decrease in groundwater flux by one order of magnitude. This is represented in the comparison between the ERT and radon fluxes for the Laguna Mouth and Oso Bay transects in which the two estimates are significantly different, as mentioned above. Groundwater sampled from shallow wells adjacent to Corpus Christi Bay exhibited an average ^{222}Rn concentration of 11,457 Bq/m³. Using the ^{222}Rn measured in the shallow wells the resulting SGD rates are almost half of estimates derived using the average porewater as the end-member (i.e. summer SGD decreased from 24 to 15 cm/d). This study uses the shallow groundwater ^{222}Rn concentrations to establish a baseline for the surrounding groundwater end-member, to compare with the time-series data, and to create a more accurate SGD rate estimate.

Data from previous studies suggest that Oso Bay is a potential contributor of higher ^{222}Rn concentrations at the Oso Bay Inlet sampling site due to the significant groundwater contribution observed further upstream (Bighash and Murgulet, 2015). In addition to these sources, surficial recirculation of water could increase observed radon concentrations and thus increase radon-based SGD estimates over those calculated using the ERT technique. Nevertheless, estimates derived from both methods yield similar trends confirming the importance of solute sources from both groundwater and recirculated waters. A 2 m^2 area was used for both techniques in estimating the volumetric discharge rates. Large differences are observed for the Oso Bay location between the ^{222}Rn -derived rates ($11.2\text{ m}^3/\text{m}\cdot\text{d}$ in summer and $15.0\text{ m}^3/\text{m}\cdot\text{d}$ in fall) and ERT rates ($0.8\text{ m}^3/\text{m}\cdot\text{d}$ in summer and $2.1\text{ m}^3/\text{m}\cdot\text{d}$ in fall). SGD volumetric rates derived for the Laguna Mouth and Shamrock Island locations vary minutely between the two methods. For the Laguna Mouth, ^{222}Rn -derived rates were slightly lower ($1.7\text{ m}^3/\text{m}\cdot\text{d}$ and $0.5\text{ m}^3/\text{m}\cdot\text{d}$) when compared to the ERT calculations ($1.8\text{ m}^3/\text{m}\cdot\text{d}$ and $1.1\text{ m}^3/\text{m}\cdot\text{d}$) while Shamrock Island had a higher ^{222}Rn -derived rate ($1.3\text{ m}^3/\text{m}\cdot\text{d}$ and $3.9\text{ m}^3/\text{m}\cdot\text{d}$) than the ER SGD rate ($0.6\text{ m}^3/\text{m}\cdot\text{d}$ and $0.8\text{ m}^3/\text{m}\cdot\text{d}$).

The rates for Shamrock Island were higher than expected, though a smaller overall flow rate comparatively. This station's far proximity to the mainland and no expected input from shoreline, suggest that these flow paths are substantially longer but are still proving to be a means of SGD. It is likely that the groundwater discharging at the Oso Bay location is more enriched in Rn or that less dilution along flow paths is occurring. Thus using the same average groundwater concentration as the end-member for all locations across the estuary may not be appropriate, resulting in more elevated SGD rates for instance at the other locations (Laguna Mouth and Shamrock Island).

3.4. Nutrient Fluxes and the Presence of Chlorophyll-a

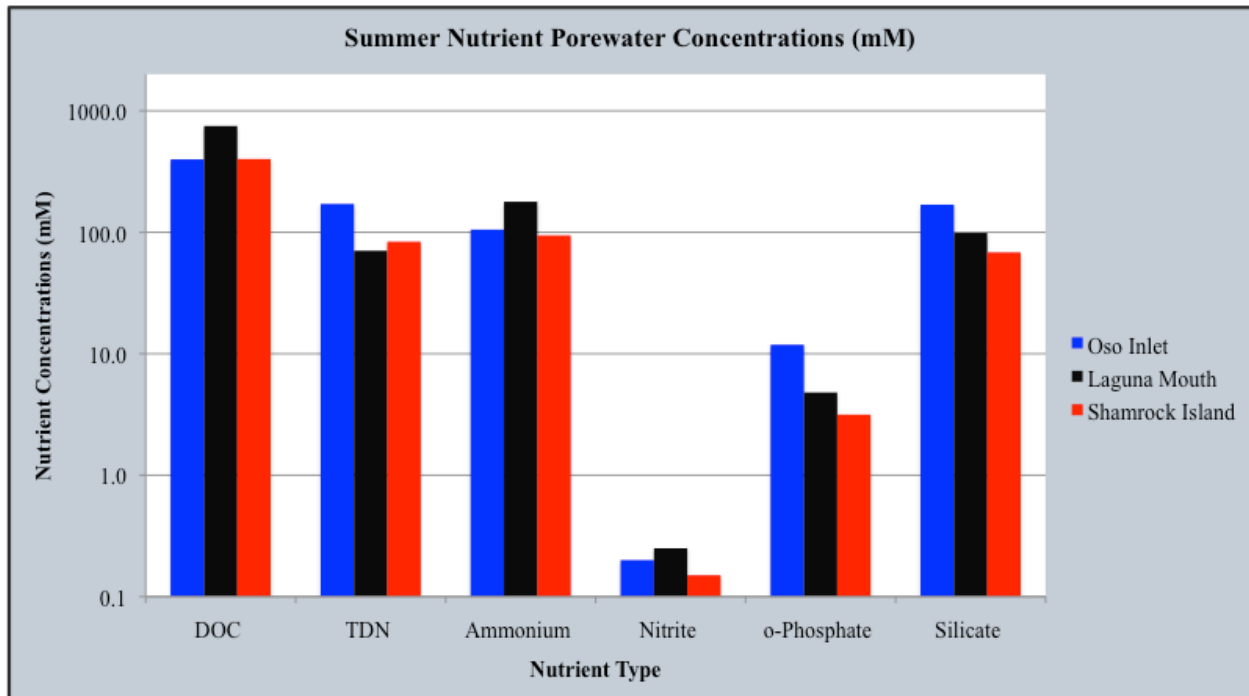


Figure 19: Summer nutrient fluxes estimated for each transect using SGD rate during the summer event, using ^{222}Rn -derived rates and porewater nutrient concentrations.

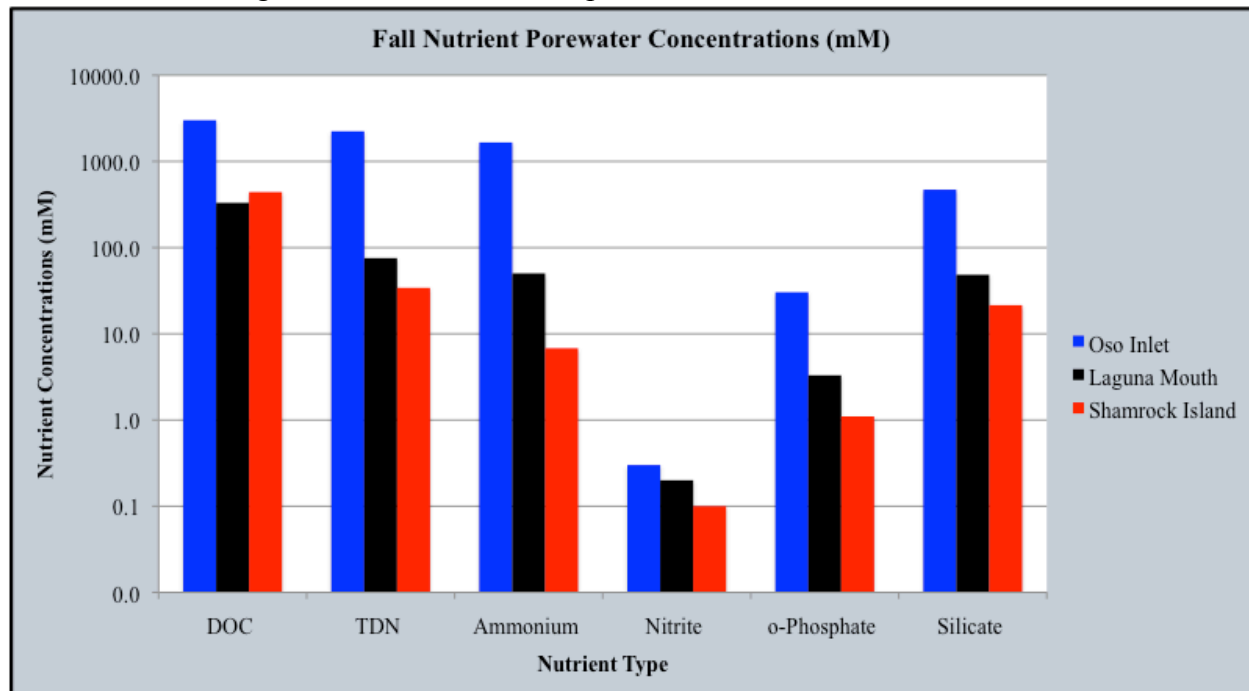


Figure 20: Fall nutrient fluxes estimated for each transect using SGD rate during the fall event, using ^{222}Rn -derived rates and porewater nutrient concentrations.

As previously stated SGD rates vary temporally and spatially, and based on the porewater nutrient data, nutrient concentrations also vary spatially and temporally. This leads to nutrient fluxes that are not only subject to changes in hydrologic conditions, but vary based on the nutrient availability. Nutrient fluxes were calculated using the ^{222}Rn -derived SGD rates multiplied by the porewater nutrient concentrations. In line with the estimated SGD data, Oso Bay inlet had the highest nutrient flux in both summer (Figure 19) and fall (Figure 20), followed by the Laguna Mouth, which had the highest nutrient concentrations, and then Shamrock Island. In fall (Figure 20) higher SGD rates are associated with an increase in nutrient fluxes by an order of a magnitude at all locations. Shamrock Island showed slightly higher fluxes in almost every category but ammonium over the Laguna Mouth, but the largest nutrient fluxes were again associated with Oso Bay. The significant increase in nutrient fluxes is not only due to SGD rates that are larger for the Oso Inlet and Shamrock Island, but due to porewater nutrient concentrations that are much more elevated for the fall event. Both nutrient and chlorophyll-a concentrations were high at Oso Bay during the fall event. On the other hand, in summer the highest chlorophyll-a concentrations were measured at the Laguna Madre and Laguna Mouth transects, followed by Oso Bay inlet. Elevated chlorophyll concentrations in the Laguna Madre during spring-summer are not uncommon even under “poor” conditions (limited rainfall, higher temperatures, and hypersaline) and similar to the collected data, concentrations tend to taper into fall and winter (Wetz, 2016). This is in large due to an extensive network of sea-grass beds found within the Upper Laguna Madre (Onuf, C.P., 1995). The presence of dense phytoplankton blooms is common along the western portion of Oso Bay (Wetz, 2014). Seasonal variations in the Oso Bay Inlet chlorophyll-a data could be a result of dilution with waters discharging from Oso Bay.

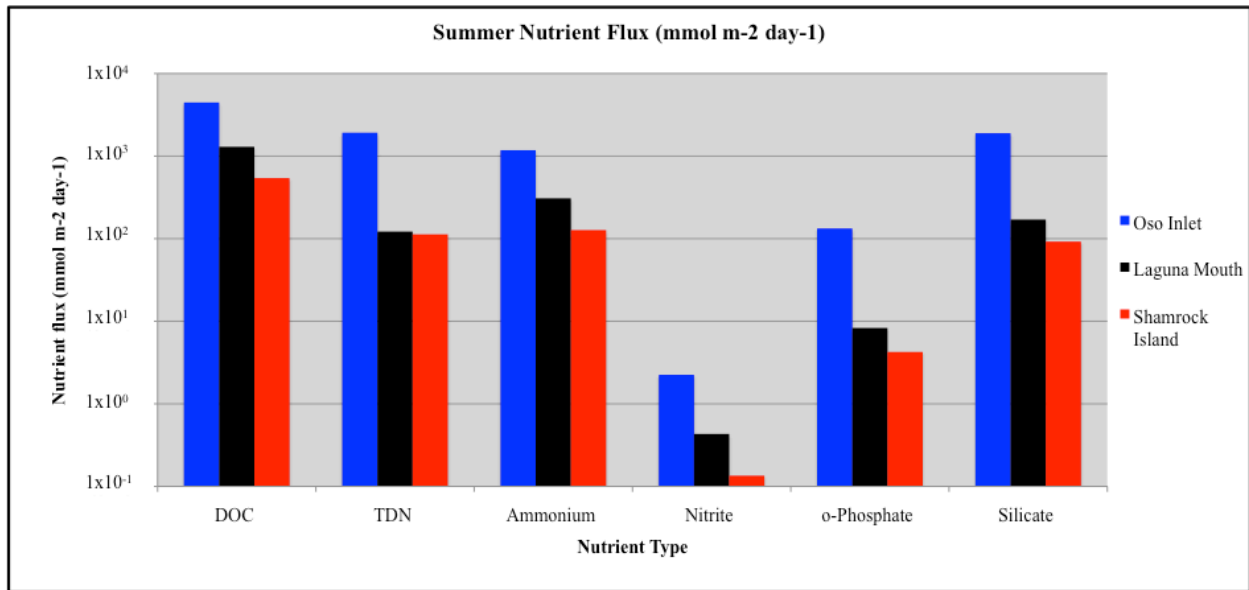


Figure 21: Summer nutrient fluxes estimated for each transect using SGD rate during the summer event, using ²²²Rn-derived rates and porewater nutrient concentrations.

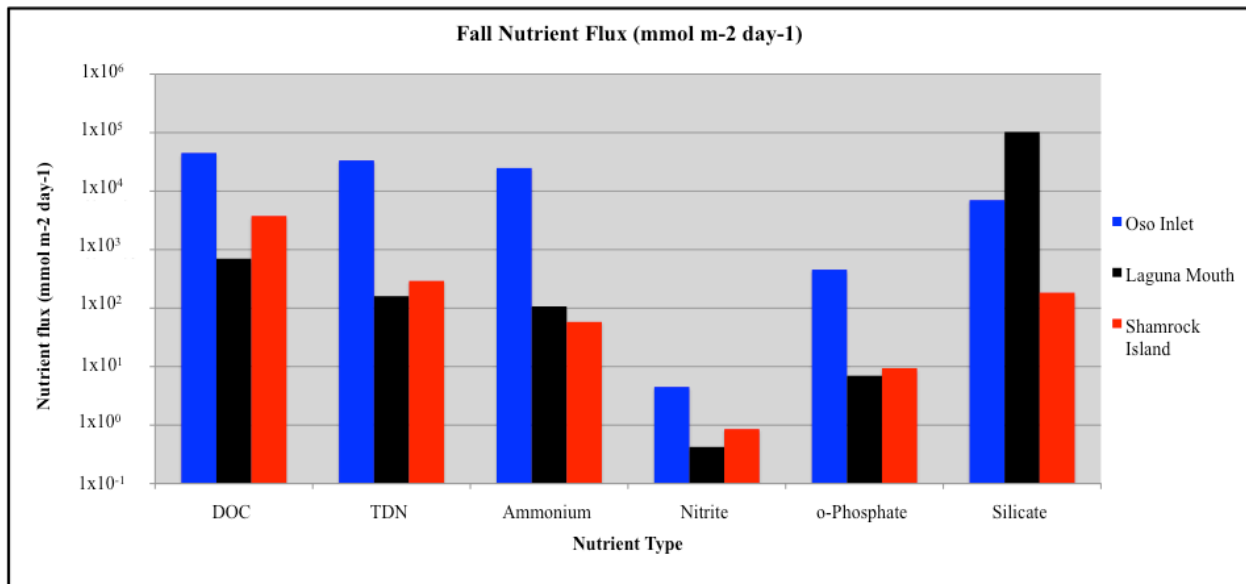


Figure 22: Fall nutrient fluxes estimated for each transect using SGD rate during the fall event, using ²²²Rn-derived rates and porewater nutrient concentrations.

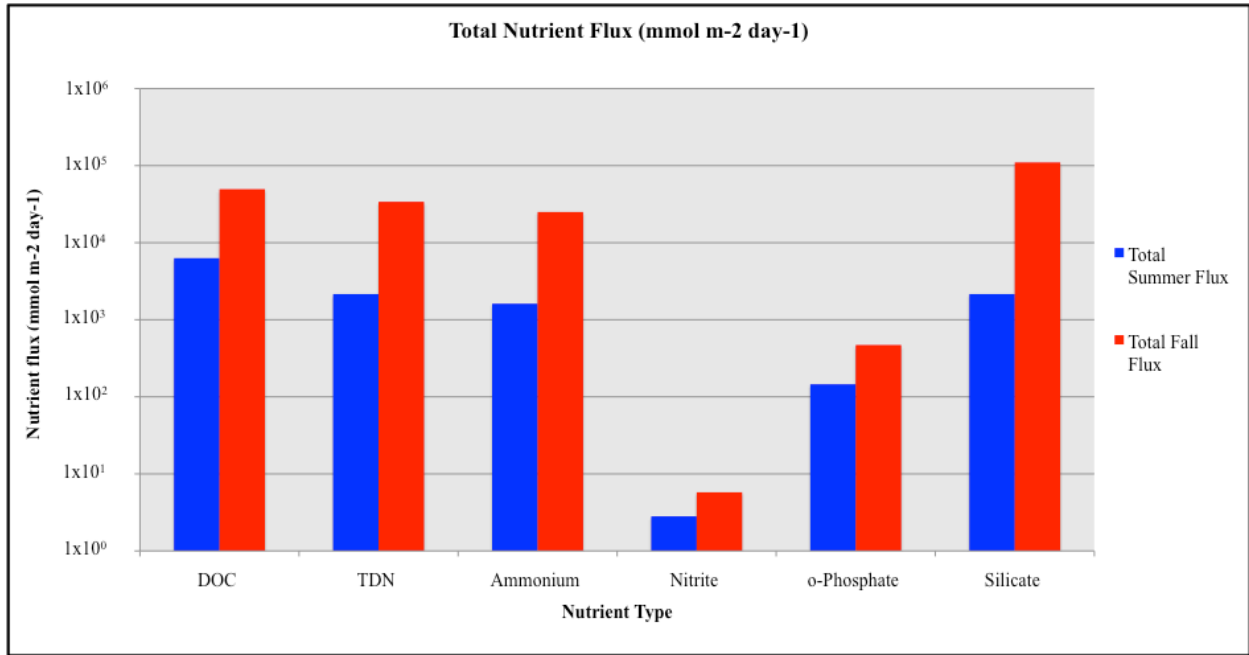


Figure 23: Total nutrient flux estimates for each season.

From the estimated SGD rates and nutrient fluxes, groundwater seems to supply a large amount of DOC, TDN, ammonium and silicate to the system during the summer and fall months.

Compared with wastewater discharge (WP) nutrient concentrations from a study done in Oso Bay (Table 2), the sampled porewater concentrations are significantly higher in DOC and ammonium (, and inline with o-phosphate (Wetz, 2014). Overall nutrient fluxes were higher in fall, despite there being a certain amount of temporal variances in nutrient concentrations at each location. This could be in relation to the higher rainfall during the fall sampling event (increasing near shore GW flow) as well as other contributing factors such as lower phytoplankton demand during fall and winter (Flint, R.W., 1984).

	DOC	Ammonium	o-Phosphate
Oso Inlet (Summer and Fall Avg)	1901	935	27.0
Oso Bay (Wastewater Discharge Avg)	383	879	58

Table 2: Comparison of nutrient concentrations between Oso Inlet porewater

averages and wastewater discharge averages (Wetz, 2014.)

Large ammonium fluxes measured in fall could be due to lower phytoplankton productivity and regeneration of organic matter in situ, as well as organic loading from seaweed and algae decay resulting in anoxic conditions (Bianchi et al., 1999; Binnerup et al., 1992).

Phytoplankton growth is generally stunted during the fall and winter (Figures 24-26) months due to a decrease in light exposure and lower temperatures, the increase in ammonium concentrations in fall (surface and porewater) could be due to this decrease in phytoplankton productivity (Kemp et al., 2005). The correlation between increased DOC and chlorophyll-a concentrations during the fall event at Oso Bay suggests both wastewater intrusion and phytoplankton exudation as a potential source, but measured nutrient fluxes suggest that SGD is a potential source that has gone unidentified and unaccounted for prior to this study (Wetz, 2014). Water column phosphate concentrations for fall are elevated in relation to summer and winter, which could be related to the higher SGD rates.

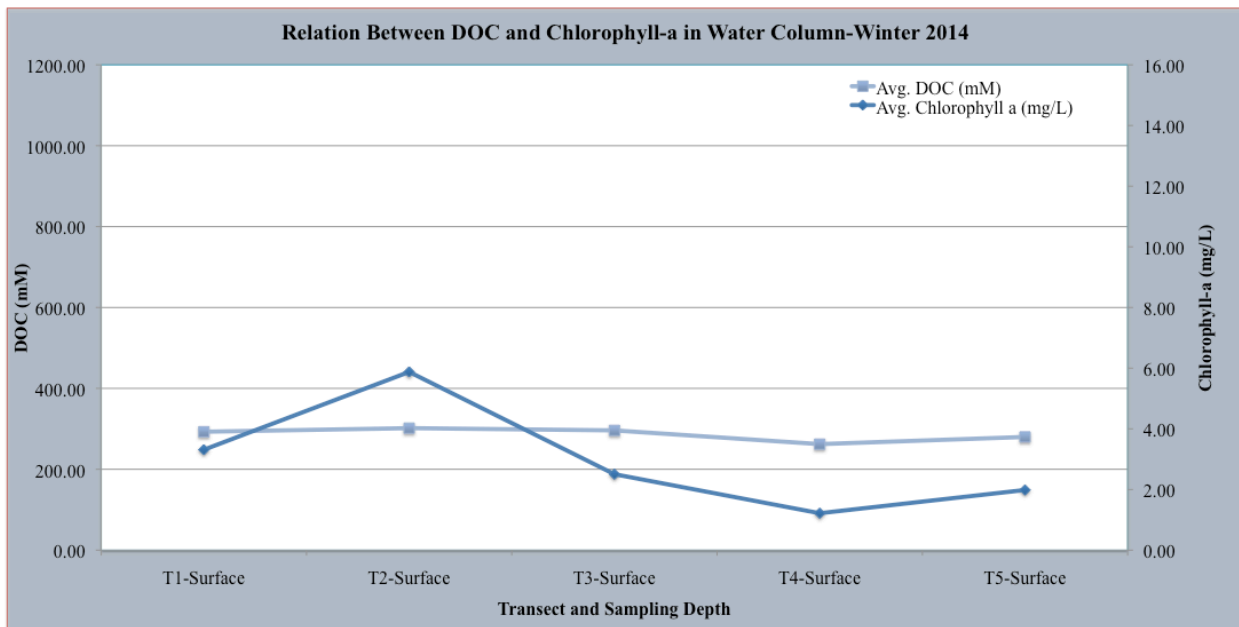


Figure 24: Relation between DOC and Chlorophyll-a in the water column during Winter 2014 (Chlorophyll-a samples were only collected at the surface during this sampling event)

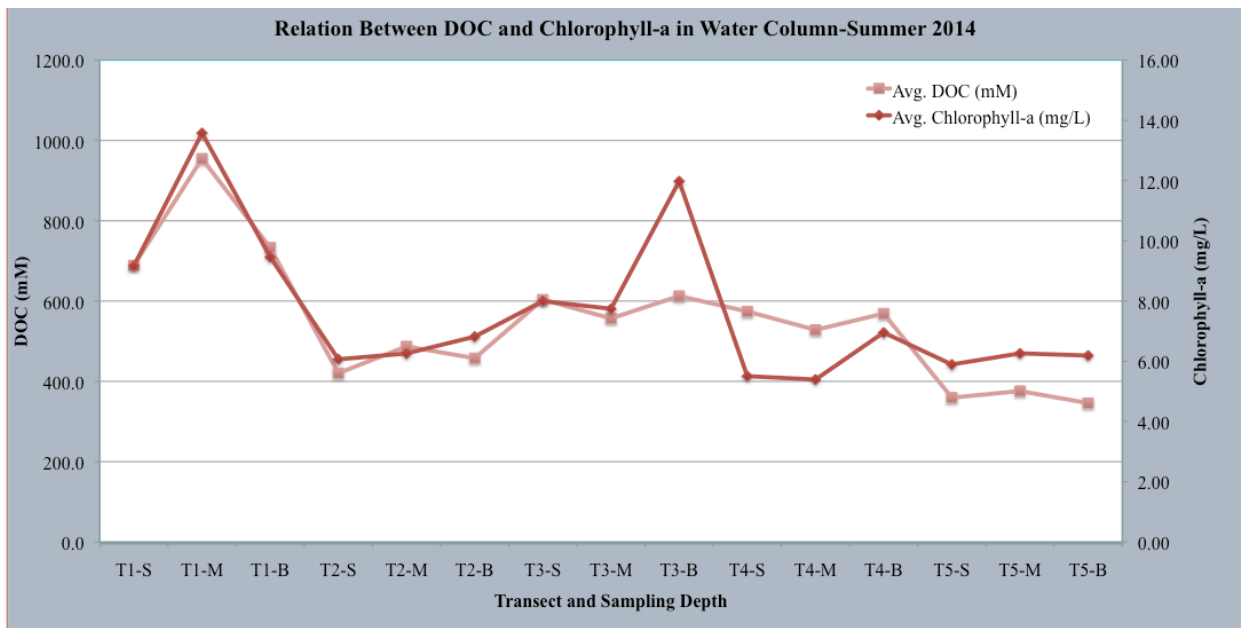


Figure 25: Relation between DOC and Chlorophyll-a in the water column during Summer 2014

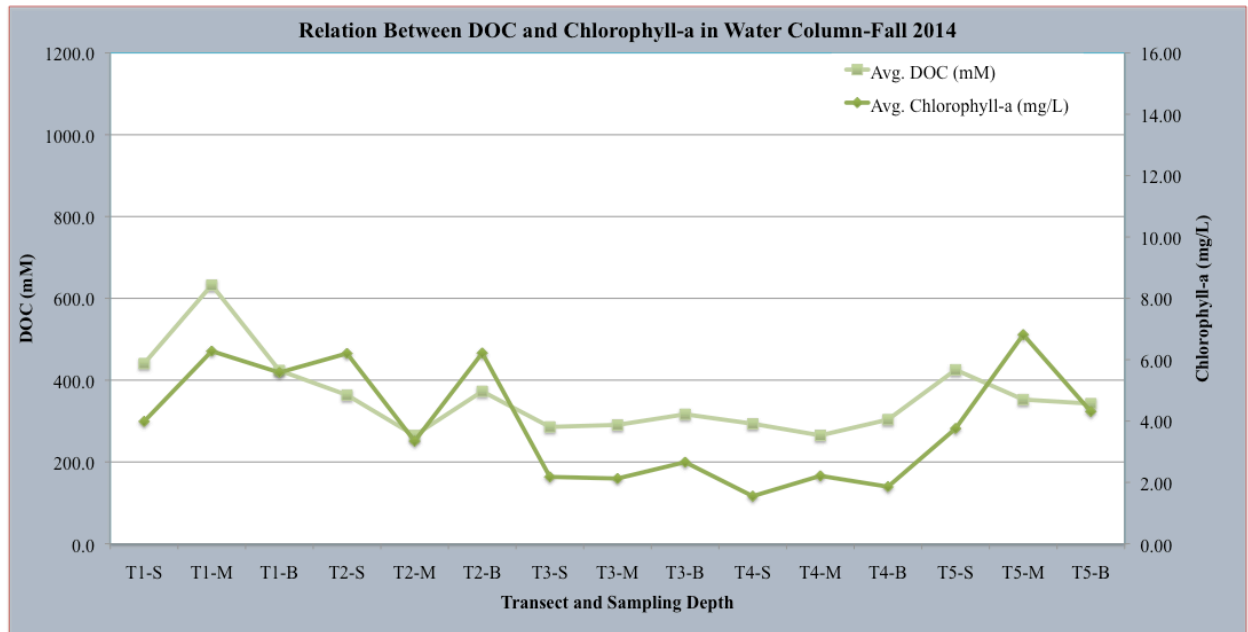


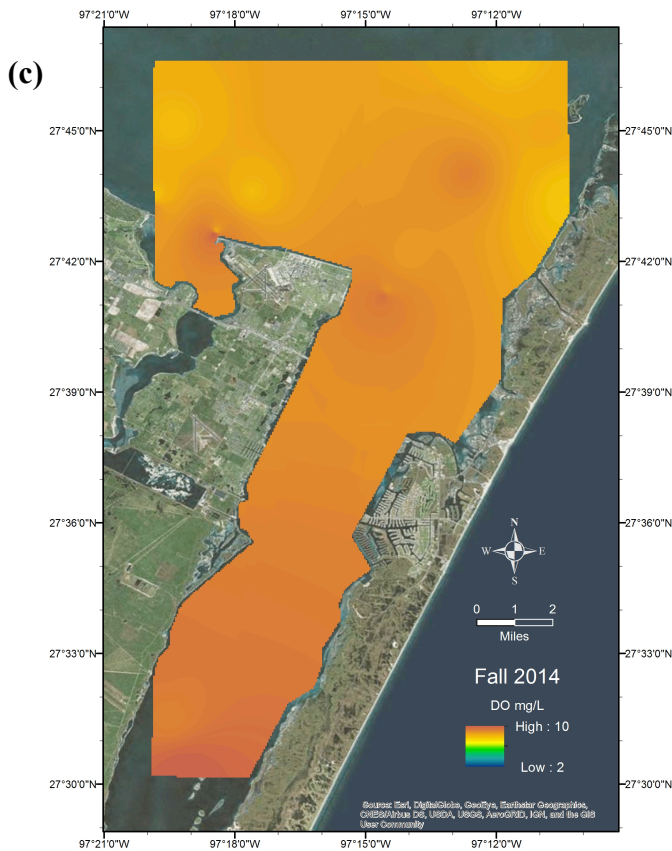
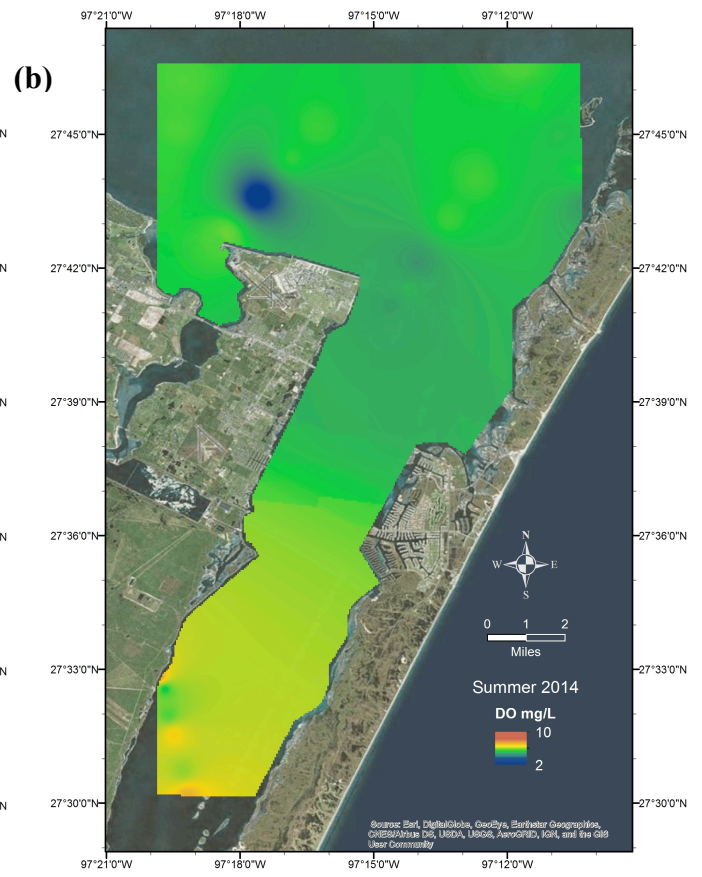
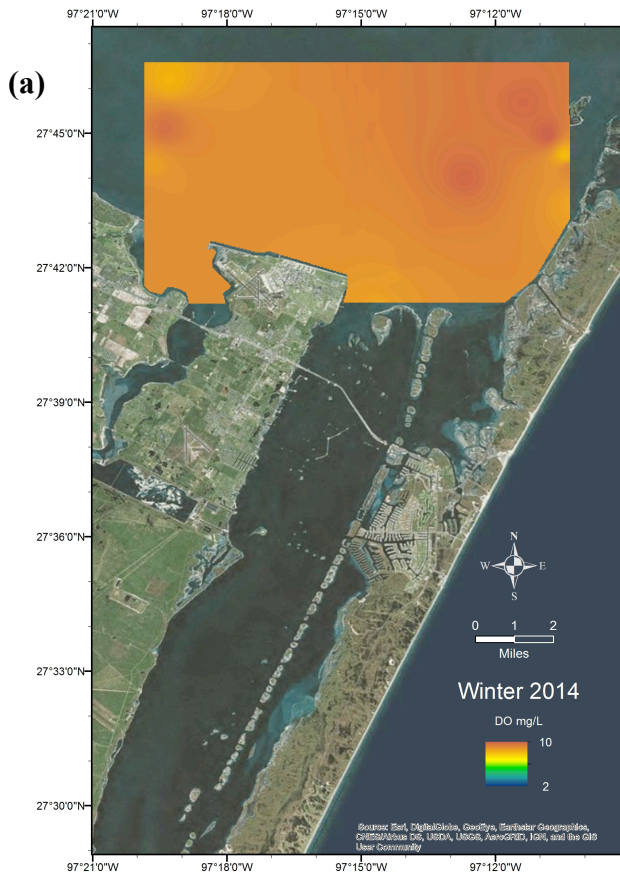
Figure 26: Relation between DOC and Chlorophyll-a in the water column during Fall 2014

Increased phosphate levels have been shown to help support algal bloom growth when combined with nitrates but alone are not a limiting factor to algal growth (Wetz, 2014). That stated, the combination of increased concentrations of both phosphate and nitrates within the porewater alludes to the significance of SGD as a source of nutrients to this estuary.

3.5. Spatial and Temporal Extent of Hypoxia

Dissolved oxygen levels for the winter and fall months show a consistent trend throughout the entire bay (Figures 27-28). Relatively speaking, the lowest DO concentrations were found near locations where SGD was found to be present. When comparing DO concentrations in the surface waters collected during the winter (8 -10.1 mg/L) and fall (7.12-8.8 mg/L) events, the summer concentrations were significantly lower at range from 1.4-8.3 mg/L. The only hypoxic DO concentration (>2 mg/L) recorded during the duration of sampling was during the summer at the bottom of the bay near the Oso Inlet. Summer has been the primary season in which hypoxia was documented to occur by Nelson and Montagna (2009) as indicated by water column and porewater DO concentrations. This has been attributed to the link between increased water temperatures and phytoplankton growth leading to hypoxia (Bissenger et al., 2009), as well as hypersaline stratification, which promotes hypoxic conditions in bottom waters (Hodges et al., 2011). Due to the large nutrient flux estimates from SGD and low DO concentrations found in the bottom waters, it is possible to link nutrient loading and the eventual eutrophication, to lower DO concentrations in these waters. The summer event also yielded the highest chlorophyll concentrations of all of the events, which would support the notion that increased algal growth is aiding in the hypoxic conditions in CCB.

Fixation of hypoxic conditions was documented to occur along the eastern portion of CCB (Nelson and Montagna, 2009). In contrast, DO concentrations from this seasonal sampling showed lower concentrations near the Oso Inlet and the Upper Laguna Madre. When comparing the two it is important to note that for this study, samples were often taken within an eight-hour sampling period and thus missing data for a complete day, which is represented in the findings from Nelson and Montagna. Spatially it is important to also note the correlation between



increased chlorophyll concentrations during the summer event and lower DO concentrations. In doing so the reflected data shows areas with connectivity to large algal blooms (Oso Inlet) and sea-grass beds (Laguna Mouth).

Figure 27: Spatial distribution of DO concentrations (mg/L) sampled from the bottom of the bay for winter (a), summer (b), and fall (c).

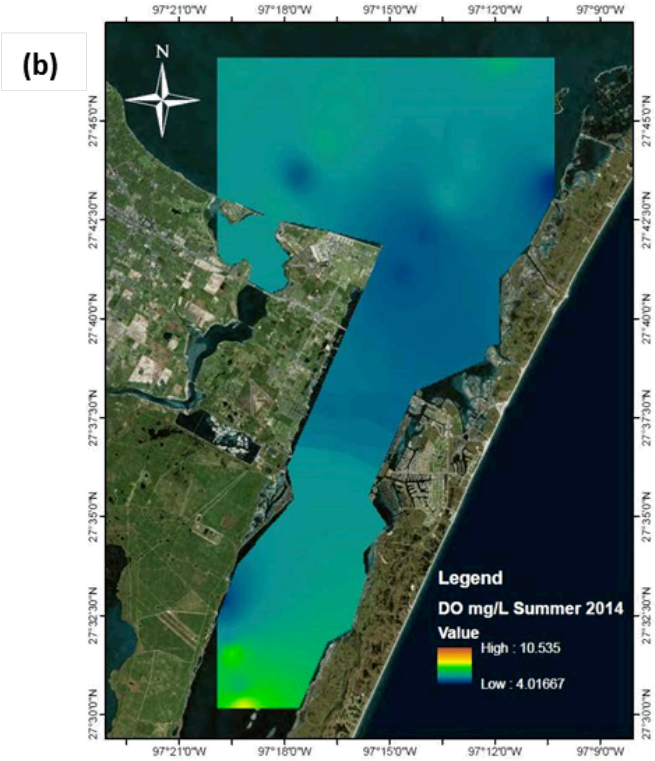
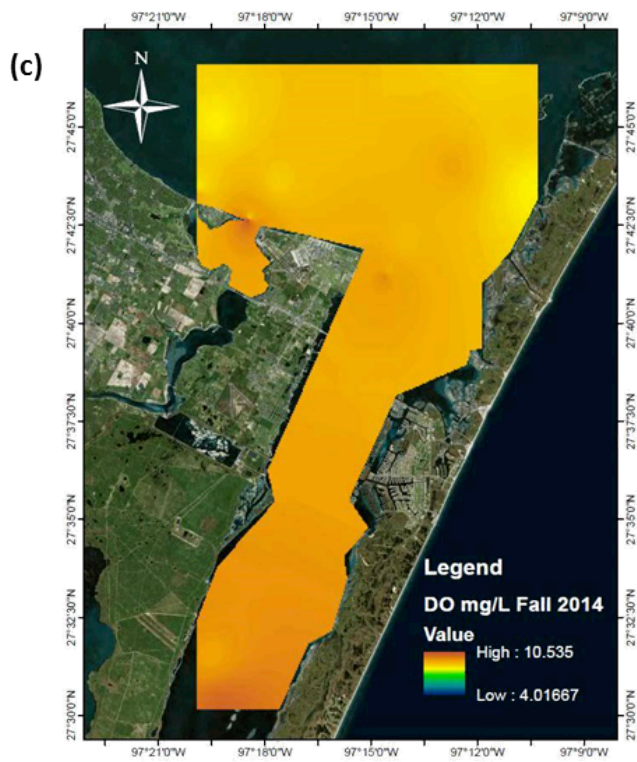
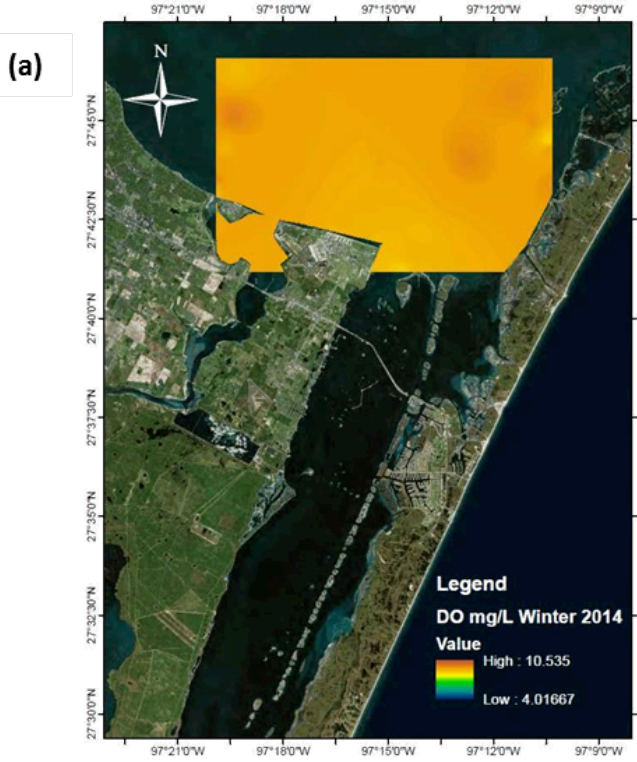


Figure 28: Spatial distribution of average water column DO concentrations (mg/L) for winter (a), summer (b), and fall (c)

4. Summary

The consistency of low inorganic nutrient and chlorophyll-a concentrations observed within the water column is the most apparent finding from the completed research. Though the influence of riverine nutrient fluxes during significant rain events and the resulting recycling of nutrients during dry spells has been well researched and documented within the south Texas bays and estuaries (Zimmerman and Benner, 1994), the potential of groundwater as a significant source to the nutrient budget has not been studied or quantified. Calculated SGD and nutrient flux rates strongly point to groundwater as a potential source of nutrients within Corpus Christi Bay.

These rates when compared to similar environments and sources prove to be substantial both as an inflow and contributor to the overall nutrient budget.

Despite the low concentrations found within the water column there are some seasonal variations observed. Surface water chlorophyll-a concentrations were highest in the summer and lowest in the winter, whereas ammonia concentrations were greater in the fall event (254.5 $\mu\text{mol/L}$) and lowest in the winter (57.1 $\mu\text{mol/L}$) and were one to two orders of magnitude greater in porewater than in the surface waters. Ammonium concentrations were highest in porewater and subsequently in the bottom water when compared to the mid water column for all seasons, and the surface samples in winter and fall. Higher NH_4 concentrations found in the porewater and bottom water suggest that sediment fluxes, though diffused, could be strong sources of NH_4 to the water column. The lowest nitrate + nitrite concentrations were found throughout the water column during the summer sampling event, which are inline with the elevated chlorophyll-a concentrations and likely a result of consumption during biomass production. Porewater nitrite concentrations are higher than the water column throughout the seasonal sampling events. TDN concentrations are also consistently higher in porewater when compared to the water column by

an order of a magnitude, with the highest concentrations being found in fall and lowest in winter. Surface water TDN concentrations were slightly elevated in the summer event when compared with the fall and winter events. In general, it is expected that the largest nutrient fluxes will occur between summer and fall and decrease with lower temperatures in winter.

Similar to ammonium, nitrite, and TDN, phosphate levels were highest in porewater samples and were an order of magnitude greater than in the water column. Silicate concentrations were consistently an order of magnitude greater in porewater when compared to the surface waters and were highest in fall (192.35 $\mu\text{mol/L}$), and the lowest in winter (67.78 $\mu\text{mol/L}$). Silicate concentrations in the water column were also lowest in the winter and during summer were almost three times higher than the average winter concentration.

Porewater ^{222}Rn concentrations were consistently an order of magnitude higher than surface waters. The average ^{222}Rn concentrations of surface water samples were twice as high in the winter when compared with the summer and fall concentrations. Although SGD fluxes were not measured for winter 2014, the higher SGD estimates derived from the continuous radon measurements at Oso Inlet and Shamrock Island for late fall, suggest that groundwater discharge rates are likely higher during the colder months. This could explain the decrease in porewater nutrient concentrations observed in winter, a result of increased SGD rates and gradual flushing of sediments.

The elevated nutrient concentrations found in porewater strongly allude to the importance of including the SGD component (including groundwater discharge and sediment fluxes) in the estimation of nutrient budgets. Summer SGD averages ranged from 1.3 to 11.2 $\text{m}^3/\text{m}\cdot\text{d}$ and the fall averaged 0.5 to 15.0 $\text{m}^3/\text{m}\cdot\text{d}$. These SGD rates translate into associated nutrient fluxes of 2.154 mol/day DIN, 6.297 mol/day of DOC, 1.329 mol/day TDN, 2.154 mol/day silicate, and

0.145 mol/day load of PO_4^{3-} per meter of bottom sediment into Corpus Christi Bay during summer. In fall these estimates increase by an order of magnitude, with 33.62 mol/day of DIN, 46.85 mol/day of DOC, 22.02 mol/day TDN, 7.132 mol/day silicate, and 0.460 mol/day load of PO_4^{3-} per meter of bottom sediment as a result of elevated porewater concentrations

The current research was conducted within an area of known hypoxic reoccurrences. With identified sites of potential SGD, it is possible to correlate SGD and hypoxia. Electrical resistivity data shows the high hydrogeologic heterogeneity of the study area, which makes it difficult to integrate the derived input loads to the entire Corpus Christi Bay system without introducing large errors. We demonstrated that by combining the ER and radon-derived methods with water-column nutrient data, that it is possible to successfully study the importance of groundwater to the overall nutrient budget and vitality of intracoastal and coastal systems. Corpus Christi Bay from a geological standpoint does not represent the ideal subsurface composition for significant interaction between the coastal aquifer and seawater. However our study has shown that even with less than ideal conditions, the potential of groundwater discharge to influence surface water chemistry by means of nutrient loading and the resulting phytoplankton respiration, though spotty, does prove to be significant. The results of this study indicate that SGD inputs associated with Oso Bay in particular, could have a significant contribution to nutrient loading and stimulation of phytoplankton growth and respiration, leading to hypoxia in the southwest corner of Corpus Christi Bay. In addition, the influence of groundwater discharge in the Upper Laguna Madre and the resulting nutrient loading could potentially play a role in brown tide outbreaks. The data from this study strongly suggests that SGD may play a significant role in the biogeochemical cycles of the Corpus Christi Bay and Upper Laguna Madre system.

5. Literature Cited

- AGI (2013). Advanced Geosciences Inc. Marine System. 2015, from <http://www.agiusa.com/marinesystem.shtml>
- Archie, G. E. (1942), The electrical resistivity logs as an aid in determining some reservoir characteristics, *Trans. AIME*, 146,54–62
- Ashworth, J. B. & Hopkins, J. (1995). *Major and minor aquifers of Texas*. (Report 345).
- Behrens, E. W., & Watson, R. L. (1973). *Corpus Christi Water Exchange Pass: a Case History of Sedimentation and Hydraulics During its First Year*. (DACW 72-72-C-0026). USDA 1992.
- Bianchi TS, Pennock JR, Twilley RR (1999) Biogeochemistry of Gulf of Mexico Estuaries, Vol. John Wiley & Sons
- Bighash, P., & Murgulet, D. (2015). Application of factor analysis and electrical resistivity to understand groundwater contributions to coastal embayments in semi-arid and hypersaline coastal settings. *Science of the Total Environment*, 532, 688-701.
- Bissenger JE, Montagnes SJ, Atkinson D. Predicting marine phytoplankton maximum growth rates from temperature: improving on the Eppley curve using quantile regression. *Limnol. Oceanogr.* 2008;53:487–493.
- Board, T. W. D. (2015). Precipitation & Lake Evaporation Data. 2015, from <http://www.twdb.texas.gov/surfacewater/conditions/evaporation/>
- Breier, J. A., Breier, C. F., & Edmonds, H. N. (2010). Seasonal dynamics of dissolved Ra isotopes in the semi-arid bays of south Texas. *Marine Chemistry*, 122(1-4), 39-50. doi: 10.1016/j.marchem.2010.08.008
- Brown, R., McClelland, N., Deininger, R., & Tozer, R. (1970). A water quality index—do we dare? *Proceedings, National Symposium on Data and Instrumentation for Water Quality Management, Volume 117*, 339-343.

- Burnett, W. C., & Dulaiova, H. (2003). Estimating the dynamics of groundwater input into the coastal zone via continuous radon-222 measurements. *Journal of Environmental Radioactivity*, 69(1-2), 21-35. doi: 10.1016/S0265-931x(03)00084-5
- Burnett, W. C., Lambert, M., & Dulaiova, H. (2001). Tracing groundwater discharge into the ocean via continuous radon-222 measurements. *Oceans 2001 Mts/Ieee: An Ocean Odyssey, Vols 1-4, Conference Proceedings*, 251-255.
- Cable, J. E., Martin, J. B., Swarzenski, P. W., Lindenberg, M. K., & Steward, J. (2004). Advection Within Shallow Pore Waters of a Coastal Lagoon, Florida. *Ground Water*, 42(7), 1011-1020. doi: 10.1111/j.1745-6584.2004.tb02640.x
- Cardenas, M. B., Zamora, P. B., Siringan, F. P., Lopus, M. R., Rodolfo, R. S., Jacinto, G. S., . . . Senal, M. I. (2010). Linking regional sources and pathways for submarine groundwater discharge at a reef by electrical resistivity tomography, Rn-222, and salinity measurements. *Geophysical Research Letters*, 37. doi: 10.1029/2010gl044066
- Church, T. M. (1996). An underground route for the water cycle. *Nature*, 380(6575), 579-580. doi: 10.1038/380579a0
- Corbett, D. R., Dillon, K., Burnett, W., & Chanton, J. (2000). Estimating the groundwater contribution into Florida Bay via natural tracers, Rn-222 and CH4. *Limnology and Oceanography*, 45(7), 1546-1557.
- Crusius, J., Koopmans, D., Bratton, J., Charette, M., Kroeger, K., Henderson, P., ... Colman, J. (2005). Submarine groundwater discharge to a small estuary estimated from radon and salinity measurements and a box model. *Biogeosciences*, 141-157.
- Department of Environmental RCRA Program SOP. 2009. Protocol for groundwater/surface water interface sampling using a pore water sampler. Benski. B.
- de Baar, H. J. W., de Jong, J. T. M., Nolting, R. F., Timmermans, K. R., van Leeuwe, M. A., Bathmann, U., . . . Sildam, J. (1999). Low dissolved Fe and the absence of diatom blooms in remote Pacific waters of the Southern Ocean. *Marine Chemistry*, 66(1-2), 1-34. doi: Doi 10.1016/S0304-4203(99)00022-5
- de Vries, J.J., Simmers, I., 2002. Groundwater recharge: an overview of processes and challenges. *Hydrogeology Journal* 10, 5–17.

- Dimova, N. T., Burnett, W. C., Chanton, J. P., & Corbett, J. E. (2013). Application of radon-222 to investigate groundwater discharge into small shallow lakes. *Journal of Hydrology*, 486, 112-122. doi: 10.1016/j.jhydrol.2013.01.043
- Dimova, N. T., Burnett, W. C., & Speer, K. (2011). A natural tracer investigation of the hydrological regime of Spring Creek Springs, the largest submarine spring system in Florida. *Continental Shelf Research*, 31(6), 731-738. doi: 10.1016/j.csr.2011.01.010
- Dimova, N. T., Swarzenski, P. W., Dulaiova, H., & Glenn, C. R. (2012). Utilizing multichannel electrical resistivity methods to examine the dynamics of the fresh water-seawater interface in two Hawaiian groundwater systems. *Journal of Geophysical Research-Oceans*, 117. doi: 10.1029/2011jc007509
- Doll, W.E., Miller, R.D., and Bradford, J. (2012). The emergence and future of near-surface geophysics. *The Leading Edge*, 31, 684-692.
- Dulaiova, H., Burnett, W.C., Chanton, J.P., Moore, W.S., Bokuniewicz, H.J., Charette, M.A., Sholkovitz, E., 2006. Assessment of groundwater discharge into West Neck Bay, New York, via natural tracers. *Continental Shelf Research* 26 (16), 1971–1983
- EPA, U. (1999). *Ecological condition of estuaries in the Gulf of Mexico*. (EPA 620-R-98-004). National Health and Environmental Effects Research Laboratory, Gulf Ecology Division, Gulf Breeze, Florida.
- Flint, R.W. (1984). Phytoplankton production in Corpus Christi Bay estuary. *Contributions in Marine Science* 27, 65-85.
- Friedel, S. (2003). Resolution, stability and efficiency of resistivity tomography estimated from a generalized inverse approach. *Geophysical Journal International*, 153(2), 305-316. doi: DOI 10.1046/j.1365-246X.2003.01890.x
- Genereux, D.P., Hemond, H.F. 1990. Naturally Occurring Radon 222 as a Tracer for Streamflow Generation: Steady State Methodology and Field Example. *Water Resources Research* 26 no 12: 3065-3075.
- Geophysics, U. O. o. G. B. o. (2013). Continuous Resistivity Profiling. Retrieved 9/1/2015, 2015, from <http://water.usgs.gov/ogw/bgas/crp/>

- Green, R.T., Winterl, J.R., Prikryl, J.D., 2008. Discharge from the Edwards aquifer through the Leona River floodplain, Uvalde, Texas. *J. Am. Water Resour. Assoc.* 44, 4 (JAWRA-07-0026-P.R1).
- Greenwood, W. J., Kruse, S., & Swarzenski, P. (2006). Extending electromagnetic methods to map coastal pore water salinities. *Ground Water*, 44(2), 292-299. doi: 10.1111/j.1745-6584.2005.00137.x
- Guo, W., Langevin, C. D., & Geological Survey (U.S.). (2002). *User's guide to SEAWAT : a computer program for simulation of three-dimensional variable-density ground-water flow*. Tallahassee, Fla.
- Johnson, T. C., Versteeg, R. J., Rockhold, M., Slater, L. D., Ntarlagiannis, D., Greenwood, W. J., & Zachara, J. (2012). Characterization of a contaminated wellfield using 3D electrical resistivity tomography implemented with geostatistical, discontinuous boundary, and known conductivity constraints. *Geophysics*, 77(6), En85-En96. doi: 10.1190/Geo2012-0121.1
- Kalke, R.D. and Montagna, P.A. 1991. The effect of freshwater inflow on macrobenthos in the Lavaca River Delta and Upper Lavaca Bay, Texas. *Contributions to Marine Science* 32:49-72.
- Kim, H. C., & Montagna, P. A. (2012). Effects of climate-driven freshwater inflow variability on macrobenthic secondary production in Texas lagoonal estuaries: A modeling study. *Ecological Modelling*, 235, 67-80. doi: 10.1016/j.ecolmodel.2012.03.022
- Krothe, J N, Garcie-Fresca, B, and Sharp, JR. J M. 2002. Effects of urbanisation on groundwater systems. 45 in Procs XXXII IAH and VI ALHSUD Congress on groundwater and human development. 21-25 October 2002. (Mar del Plata, Argentina: Univ National de Mar del Plata.)
- Lee, M. W., & Collett, T. S. (2006). Gas hydrate and free gas saturations estimated from velocity logs on Hydrate Ridge, offshore Oregon, USA. *Proc. Ocean Drill. Program Sci. Results*, 204, 1-25. doi: 10.2973

- Li, H., & Jiao, J. (2013). Quantifying tidal contribution to submarine groundwater discharges: A review. *Chinese Science Bulletin*, 58(25).
- Loke, M. H. (2011), Tutorial: 2-D and 3-D electrical imaging surveys, Geotomo Software Sdn. Bhd., Penang, Malaysia.
- MacIntyre, S., Wanninkhoe, R., & Chanton, J. P. (1995). Trace gas exchange across the air-water interface in freshwaters and coastal marine environments. 52-57.
- Martin, C.M. and P.A. Montagna. 1995. Environmental assessment of La Quinta Channel, Corpus Christi Bay, Texas. *Texas Journal of Science* 47:203-222.
- Montagna, P. A., & Froeschke, J. (2009). Long-term biological effects of coastal hypoxia in Corpus Christi Bay, Texas, USA. *Journal of Experimental Marine Biology and Ecology*, 381, S21-S30. doi: 10.1016/j.jembe.2009.07.006
- Montagna, P. A., & Ritter, C. (2006). Direct and indirect effects of hypoxia on benthos in Corpus Christi Bay, Texas, USA. *Journal of Experimental Marine Biology and Ecology*, 330(1), 119-131. doi: 10.1016/j.jembe.2005.12.021
- Moore, W. S. (1996). Large groundwater inputs to coastal waters revealed by Ra-226 enrichments. *Nature*, 380(6575), 612-614. doi: Doi 10.1038/380612a0
- Moore, W. S. (2000). Determining coastal mixing rates using radium isotopes. *Continental Shelf Research*, 20(15), 1993-2007. doi: Doi 10.1016/S0278-4343(00)00054-6
- Morehead, S., Montagna, P., & Kennicutt, M. C. (2008). Comparing fixed-point and probabilistic sampling designs for monitoring the marine ecosystem near McMurdo Station, Ross Sea, Antarctica. *Antarctic Science*, 20(5), 471-484. doi: 10.1017/S0954102008001326
- Morell, I., Gimenez, E., & Esteller, M. V. (1996). Application of principal components analysis to the study of salinization on the Castellon Plain (Spain). *Science of the Total Environment*, 177, 161-171. doi: 10.1016/0048-9697(95)04893-6
- Murgulet, D., & Tick, G. R. (2015). Nitrate Flux to Coastal Waters in Response to Variable-Density Groundwater Flow. . *Journal of Hydrological Processes [In Press]*

- Murray, J. (2004). Major Ions of Seawater. 2015, from http://www.ocean.washington.edu/courses/oc400/Lecture_Notes/CHPT4.pdf
- Nelson, K. M., P. A. (2009). Causes and Monitoring of Hypoxia in Corpus Christi Bay. Coastal Bend Bays & Estuaries Program.
- Ni, S. B., W. C., Eller, K. T., Macintyre, H. L., Mortazavi, B., Liefer, J. D., & Novoveska, L. (2011). Radon and Radium isotopes, groundwater discharge and harmful algal blooms in Little Lagoon, Alabama. *Interdisciplinary Studies on Environmental Chemistry-Environmental Pollution and Ecotoxicology*, 329-337.
- NOAA. (2014). National Oceanic and Atmospheric Administration's, National Weather Service. 2015, from <http://www.ncdc.noaa.gov>
- Nyquist, J. E., Freyer, P. A., & Toran, L. (2008). Stream bottom resistivity tomography to map ground water discharge. *Ground Water*, 46(4), 561-569. doi: 10.1111/j.1745-6584.2008.00432.x
- Onuf, C.P., 1995, Seagrass meadows of the Laguna Madre of Texas, *in* LaRoe, E.T., Farris, G.S., Puckett, C.E., Doran, P.D., and Mac, M.J., eds., Our living resources: a report to the Nation on the distribution, abundance, and health of U.S. plants, animals, and ecosystems: Washington, D.C., U.S. Department of the Interior, National Biological Service, p. 275–277.
- Rajmohan, N., & Elango, L. (2005). Nutrient chemistry of groundwater in an intensively irrigated region of Southern India. *Environmental Geology*, 47, 820–830.
- RCRA SOP, 2009. Protocol for Groundwater/Surface Water Interface Sampling Using a Pore Water Sampler. Department of Environmental Protection Bureau of Remediation and Waste Management RCRA Program.
- Ritter, C., & Montagna, P. A. (1999). Seasonal hypoxia and models of benthic response in a Texas bay. *Estuaries*, 22(1), 7-20. doi: Doi 10.2307/1352922
- Samouelian, A., Cousin, I., Tabbagh, A., Bruand, A., & Richard, G. (2005). Electrical resistivity survey in soil science: a review. *Soil & Tillage Research*, 83(2), 173-193. doi: 10.1016/j.still.2004.10.004

- Selman, M., S. Greenhalgh, R. Diaz, and Z. Sugg. 2008. *Eutrophication and Hypoxia in Coastal Areas: A Global Assessment of the State of Knowledge*. Water Quality: Eutrophication and Hypoxia Policy Note Series No.1. Washington, DC: World Resources Institute.
- Sugita, F., Nakane, K., 2007. Combined effects of rainfall patterns and porous media properties on nitrate leaching. *Vadose Zone Journal* 6, 548.
- Thareja, S., Choudhury, S., & Trivedi, P. (2011). Assessment of water quality of Ganga River in Kanpur by using principal components analysis. *Advances in Applied Science Research*, 2(5), 84-911.
- Turner, R.E., Rabalais, N.N., and Justić, Dubravko, 2008, Gulf of Mexico hypoxia—Alternate states and a legacy: *Environmental Science and Technology*, v. 42, no. 7, p. 2323-2327.
- U.S. Census Bureau. (2014). State and County Quick Facts: Corpus Christi (city) Texas. U.S. Department of Commerce. Retrieved from <http://quickfacts.census.gov/qfd/states/35/3564930>
- USDA. 1992. Soil Survey, Nueces County Texas. United States Department of Agriculture Soil Conservation Service Report. 64 pp. + maps.
- USEPA. 1999. Ecological condition of estuaries in the Gulf of Mexico. EPA 620-R-98-004. U.S. Environmental Protection Agency, Office of Research and Development, National Health and Environmental Effects Research Laboratory, Gulf Ecology Division, Gulf Breeze, Florida. 80 pp.
- Verity, P.G., M. Alber, and S.B. Bricker. 2006. Development of hypoxia in well-mixed subtropical estuaries in the southeastern U.S.A. *Estuaries and Coasts* 29: 665-673
- Viso, R., C. McCoy, P. Gayes, and D. Quafisi (2010), Geological control on submarine groundwater discharge in Long Bay, South Carolina (USA), *Cont. Shelf Res.*, 30, 335–341, doi:10.1016/j.csr.2009.11.014.
- Waterstone. (2003). *Groundwater availability of the central Gulf Coast aquifer—Numerical simulations to 2050, Central Gulf Coast, Texas*. Texas Water Development Board, Austin, Texas, variously paginated.

- Wetz, M.S. (2014). Evaluation of factors contributing to water quality degradation in an urbanizing estuary (Oso Bay, Texas). GLO Contract (13-036-000-6903).
Texas General Land Office Austin, TX
- White, P. A. (1988). Measurement of Groundwater Parameters Using Salt-Water Injection and Surface Resistivity. *Ground Water*, 26(2), 179-186. doi: 10.1111/j.1745-6584.1988.tb00381.x
- Wood, W. W. (1976). *Guidelines for collection and field analysis of ground-water samples for selected unstable constituents*. Techniques of Water Resources Investigation, Book 1, Ch D2: Retrieved from <http://pubs.usgs.gov/twri/twri1-d2/>.
- X. Li, B.X. Hu, W.C. Burnett, I.R. Santos, J.P. Chanton Submarine ground water discharge driven by tidal pumping in a heterogeneous aquifer *Ground Water*, 47 (2009), pp. 558–568 doi: 10.1111/j.1745-6584.2009.00563.
- Zimmerman, A. R., and Benner, R.. 1994. Denitrification, nutrient regeneration and carbon mineralisation in sediments of Galveston Bay, Texas, USA. *Mar. Ecol. Prog. Ser.* **114**: 275– 288.

6. Appendix 6.1.

Nutrient Data

	DOC (mM)	TDN (mM)	Ammonium (mM)	Nitrite (mM)	o-Phosphate (mM)	Silicate (mM)
Oso Inlet	397.9	171.3	105.2	0.2	11.9	168.8
Laguna Mouth	750.3	70.6	178.4	0.3	4.8	98.7
Shamrock Island	401.1	83.7	94.2	0.2	3.2	68.3

Table N6-1: Summer nutrient concentrations

	DOC (mM)	TDN (mM)	Ammonium (mM)	Nitrite (mM)	o-Phosphate (mM)	Silicate (mM)
Oso Inlet	3006.3	2235.5	1660.0	0.3	30.4	469.5
Laguna Mouth	330.9	75.6	50.3	0.2	3.3	48.5
Shamrock Island	440.8	34.2	6.8	0.1	1.1	21.5

Table N6-2: Fall nutrient concentrations

	DOC (mmol m ⁻² day ⁻¹)	TDN (mmol m ⁻² day ⁻¹)	Ammonium (mmol m ⁻² day ⁻¹)	Nitrite (mmol m ⁻² day ⁻¹)	o-Phosphate (mmol m ⁻² day ⁻¹)	Silicate (mmol m ⁻² day ⁻¹)
Oso Inlet	4459.7	1919.4	1178.5	2.2	132.8	1891.4
Laguna Mouth	1296.4	121.9	308.3	0.4	8.3	170.6
Shamrock Island	540.6	112.8	127.0	0.1	4.2	92.1
Total	6296.7	2154.1	1613.8	2.8	145.4	2154.0

Table N6-3: Summer nutrient flux estimates

	DOC (mmol m-2 day-1)	TDN (mmol m-2 day-1)	Ammonium (mmol m-2 day-1)	Nitrite (mmol m-2 day-1)	o-Phosphate (mmol m-2 day-1)	Silicate (mmol m-2 day-1)
Oso Inlet	44986.3	33452.0	24840.2	4.5	454.2	7024.8
Laguna Mouth	701.5	160.3	106.6	0.4	7.0	102820.0
Shamrock Island	3765.3	291.7	58.1	0.9	9.4	183.7
Total	49453.1	33904.0	25005.0	5.8	470.5	110028.5

Table N6-4: Fall nutrient flux estimates

	DOC (mmol m-2 day-1)	TDN (mmol m-2 day-1)	Ammonium (mmol m-2 day-1)	Nitrite (mmol m-2 day-1)	o-Phosphate (mmol m-2 day-1)	Silicate (mmol m-2 day-1)
Total Summer Flux	6296.7	2154.1	1613.8	2.8	145.4	2154.0
Total Fall Flux	49453.1	33904.0	25005.0	5.8	470.5	110028.5

Table N6-5: Nutrient flux estimated totals for summer and fall